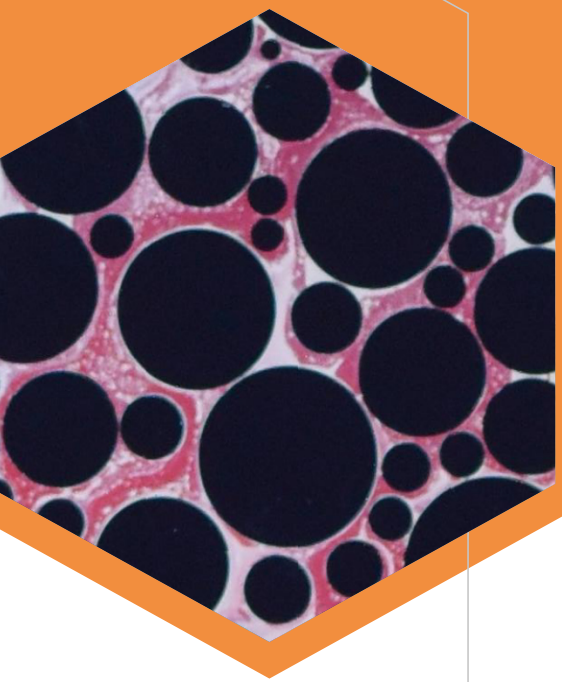

844

Research Report

Experimental Analysis of Conformance Control Methods
Shut-Off Mechanisms for Water Flow in Reservoirs

Umschlaggestaltung: DIE NEUDENKER®, Darmstadt | DGMK e.V., Hamburg
Titelfotografie: TU Clausthal

ISSN 0937-9762
ISBN 978-3-947716-51-7

https://www.dgmk.de

DGMK-Research Report 844

Experimental Analysis of Conformance Control Methods
Shut-Off Mechanisms for Water Flow in Reservoirs

Abstract

In this project DGMK 844, the previous research on conformance control was expanded to include the method of microfluidics. In the first part of the project, the findings on and around conformance control were brought up to date in an intensive literature search. In the second work package, new micromodels were designed and manufactured. These exhibit features in their structure commonly found in reservoirs with degraded conformance. One edition of the models has fractures in its structure, while another has layers of high and low permeability. Various products such as polymers, gels and so-called Relative Permeability Modifiers (RPMs) are used to mitigate conformance problems. Examples of this are used in work packages 3 and 4 both in core floods and in micromodels.

Length of the report:	78 pages, 51 figures, 22 tables
Duration:	01.07.2020 - 31.01.2023
Research Scientists:	Prof. L. Ganzer, M.Sc. S. Säfken, Dr.-Ing. C. L. Gaol TU Clausthal: Institute of Subsurface Energy Systems (ITE)
Project Advisors:	W. Jelinek, A. Fodgen, A. Kasprzak, H. Vorholt, Wintershall Dea, Barnstorf G. Ionescu, ExxonMobil Production Deutschland GmbH, Hannover T. Mozer, Neptune Energy Deutschland GmbH, Lingen A. Gobi, Vermillion Energy Deutschland GmbH & Co. KG, Hannover -
Project Coordination:	Dr. Susanne Kuchling, DGMK e.V., Hamburg
DGMK-Technical Commitee:	Production Engineering
Published:	Hamburg, February 2023

DGMK-Forschungsbericht 844

Experimentelle Analysen von, Conformance-Control' Methoden
Absperrmechanismen für den Wasserfluss in Stauseen

Kurzfassung

In diesem Projekt DGMK 844 wurde die bisherige Forschung zu Conformance Control um die Methode der Mikrofluidik erweitert. Im ersten Teil des Projektes wurden in einer intensiven Literaturrecherche die Erkenntnisse zu und um Conformance Control auf einen aktuellen Stand gebracht. Im zweiten Arbeitspaket wurden neue Mikromodelle entworfen und hergestellt. Diese weisen in ihrer Struktur Merkmale auf, die häufig in Lagerstätten mit Konformitätseinbußen zu finden sind. So hat eine Auflage der Modelle Risse in ihrer Struktur, während eine andere hoch und niedrig permeable Schichten aufweist. Zur Minderung der Konformitätsprobleme werden verschiedene Produkte wie Polymere, Gele und sogenannte Relative Permeability Modifier (RPMs) eingesetzt. Beispiele hierfür werden in den Arbeitspaketen 3 und 4 sowohl in Kernfluten als auch in Mikromodellen angewendet.

Berichtsumfang:	78 Seiten, 51 Abbildungen, 22 Tabellen
Laufzeit:	01.07.2020 – 31.01.2023
Projektbearbeiter:	Prof. L. Ganzer, M.Sc. S. Säfken, Dr.-Ing. C. L. Gaol TU Clausthal: Institute of Subsurface Energy Systems (ITE)
Projektbegleitung:	Dr. T. Bartels, Dr. J. Nüchter, Wintershall Dea, Hamburg
	K. Müller, ExxonMobil Production Group Deutschland GmbH, Hannover
	K. Krause, Neptune Energy Deutschland GmbH, Lingen
	K. Flechter, Vermilion Energy GmbH
Projektkoordination:	Dr. Susanne Kuchling, DGMK e.V., Hamburg
DGMK-Fachausschuss:	Fördertechnik
Veröffentlichung:	Hamburg, Februar 2023

Table of contents

Abstract ... ii
Kurzfassung ... iii
List of Tables ... vi
List of Figures ... vii
1. Executive summary ... 1
2. Zusammenfassung ... 2
3. Introduction ... 3
4. Methodology ... 4
4.1 Minutes for experimental work from Kick-Off ... 4
4.2 Rheology ... 5
4.3 Fluids ... 6
4.3.1 Oil ... 7
4.3.2 Brine ... 9
4.3.3 Other aqueous salt solutions ... 9
4.4 Rock samples ... 10
4.4.1 Bentheimer ... 10
4.4.2 Dogger ß ... 13
5. Work Package – 1 Selection of Products and Literature Update ... 14
5.1 Literature Update ... 14
5.1.1 Improvement of Stability ... 15
5.1.2 Reduction of Environmental Impact ... 20
5.1.3 Future Trends ... 22
5.2 Investigated Products – Properties, Application and Working Mechanisms ... 23
5.2.1 H_2Zero™ ... 23
5.2.2 FormSeal ... 29
5.2.3 PowelGel M2ES ... 34
5.2.4 PowelGel M2EMC ... 37
5.2.5 WaterWeb® ... 39
5.2.6 LCH5198B ... 40
5.2.7 EBO5284B ... 42
6. Work Package – 2 Selection of Products and Literature Update ... 43
6.1 Source rock ... 43
6.2 Image processing ... 43
6.2.1 High and low permeable strata model ... 44
6.2.2 Fractured micromodel ... 44
6.2.3 Final models ... 45
7. Work Package – 3 Core flooding experiments ... 49
7.1 WaterWeb ... 50

7.2 Form Seal 51
7.3 M2ES 51
7.4 M2EMC 53
7.5 H2Zero™ 54
7.6 EBO5284B 54
7.7 LCH5198-B 54
7.8 Summary of core flooding experiments 55
8. Work Package – 4 Microfluidic experiments 56
8.1 WaterWeb single-phase flow 56
8.2 M2ES single-phase flow 57
8.3 M2EMC single-phase flow 59
8.4 LCH5198 single-phase flow 60
8.5 WaterWeb two-phase flow 61
8.6 Summary of microfluidic experiments 64
9. Conclusion 65
References 66
Abbreviations 70
Symbols and units 71
Appendix 73

List of Tables

Table 1: Time schedule and Gantt chart of the DGMK 844 project 1
Table 2: Time schedule and Gantt chart of the DGMK 844 project 2
Table 3: Viscosity of dead oil at different temperatures 7
Table 4: Viscosity of dead oil thinned with n-decane at different proportions at room temperature 8
Table 5: Viscosity of dead oil 8
Table 6: Brine composition 9
Table 7: Viscosity of H2Zero™ reactants 25
Table 8: Viscosity of H2Zero™ during gelation – Part I 26
Table 9: Gel strength of H_2Zero™ 27
Table 10: Viscosity alteration of H2Zero™ during gelation – Part II 28
Table 11: Viscosity of Gascon 469 30
Table 12: Viscosity of FormSeal during gelation at 45°C – 1st measurement 30
Table 13: Viscosity of FormSeal during gelation at 45°C – 2nd measurement 31
Table 14: Viscosity of FormSeal during gelation at 55 ◦C 32
Table 15: Viscosity of M2ES of stock solutions 36
Table 16: Viscosity of M2ES 1156 ppm solutions 36
Table 17: Viscosity of M2EMC stock solutions 38
Table 18: Viscosity of M2EMC 1434 ppm solutions 39
Table 19: Results from Water Web core flooding experiments 50
Table 20: Results from Form Seal core flooding experiments 51
Table 21: Results from all core flooding experiments 55
Table 22: Results from all microfluidic flooding experiments 64
*Table 23: **A1:** Gel strength by Sydansk* 73

List of Figures

Figure 1: Rheometer geometries 6
Figure 2: Dead oil at different temperatures 7
Figure 3: Viscosity of dead oil thinned with n-decane at different proportions 8
Figure 4: Viscosity of dead oil thinned dead oil 8
Figure 5: Provided core material 10
Figure 6: Provided BH cores after drilling of small cores 11
Figure 7: BH cores for µCT-imaging in Soxhlet top piece 12
Figure 8: Soxhlet apparatus 12
Figure 9: Number of publications linked to specific keywords over time 14
Figure 10: Viscosity of H2Zero™ reactants 25
Figure 11: Viscosity alteration of H_2Zero™ during gelation – Part 26
Figure 12: Viscosity alteration of H_2Zero™ during gelation – Part II 28
Figure 13: Viscosity alteration of H2Zero™ during gelation (pre-sheared samples) 28
Figure 14: Viscosity of Gascon 469 30
Figure 15: Viscosity alteration of FormSeal during gelation at 45 ◦C – 1st measurement 30
Figure 16: Viscosity alteration of FormSeal during gelation at 45 ◦C–2nd measurement 31
Figure 17: Viscosity alteration of FormSeal during gelation at 55 ◦C 32
Figure 18: Gelation experiment with FormSeal 34
Figure 19: Viscosity of M2ES stock solution prepared with different brines 35
Figure 20: Viscosity of M2ES 1156 ppm solution prepared with different brines 36
Figure 21: Viscosity of M2EMC stock solution prepared with different brines 38
Figure 22: Viscosity of M2EMC 1434 ppm solution prepared with different brines 38
Figure 23: Rheology of LCH5198B and EBO5284B in 60 kppm brine 40
Figure 24: Rheology of LCH5198B in 100kppm brine 41
Figure 25: Rheology of LCH8198B 41
Figure 26: Rheology of EBO5284B 42
Figure 27: Steps of porous structure design 44
Figure 28: Visualisation of fracture generation in MatLab®. 45
Figure 29: All available designs of micromodels based on µCt images of Dogger β sandstone – Homogeneous matrix (top),[33] heterogeneous structure with high and low permeable strata (middle) and fractures structure (bottom) 46
Figure 30: All available designs of micromodels based on µCt images of Bentheimer sandstone – Homogeneous matrix (top),[33] heterogeneous structure with high and low permeable strata with higher difference as published by Gaol et al. (middle) and fractures structure (bottom) 46
Figure 31: Bentheimer micromodels – Homogeneous matrix (top),[33] heterogeneous structure with high and low permeable strata with higher difference as published by Gaol[33] (middle) and fractured structure (bottom). 47
Figure 32: Realistic micromodels with fractures of different widths 47
Figure 33: Permeability measurements in fractured Bentheimer micromodel 48
Figure 34: Permeability measurements in fractured Bentheimer micromodel with high and low permeable strata 48
Figure 35: Core flooding setup 50
Figure 36: Permeability measurements before and after application of M2ES – Experiment I 52
Figure 37: Permeability measurements before and after application of M2ES – Experiment II 52
Figure 38: Permeability measurements before and after application of M2EEMC – Experiment I 53
Figure 39: Permeability measurements before and after application of M2EMC – Experiment II 53
Figure 40: Permeability measurement after treatment with LCH5198-B 55
Figure 41: Results from microfluidic experiment with WaterWeb 56
Figure 42: Image of focus micromodel area obtained with objective 5x Brightfield transmitted light (left) and objective 40x Brightfield transmitted light (right) 57
Figure 43: Permeability measurements before and after application of M2ES – Experiment in fractured micromodel 58
Figure 44: Permeability measurements before and after application of M2ES – Experiment in high and low permeable micromodel 58

Figure 45: Permeability measurements before and after application of M2EMC – Experiment in fractured micromodel 59
Figure 46: Permeability measurements before and after application of M2EMC– Experiment in high and low permeable micromodel 59
Figure 47: Permeability measurements before and after application of LCH5198– Experiment in fractured micromodel 60
Figure 48: Permeability measurements before and after application of LCH5198– Experiment in high and low permeable micromodel 60
Figure 49: Images of two-phase flow microfluidic experiment with WaterWeb 62
Figure 50: The capillary desaturation curve (left) and end-point water relative permeability relationship to capillary number. 63
Figure 51: Permeability measurements before and after application of WaterWeb in two phase flooding experiment 63

1. Executive summary

In this project DGMK 844, the previous research on conformance control was expanded to include the method of microfluidics. The project was scheduled to extend over 24 months in total from July 2020 to June 2022 (Table 1). It was extended for another seven months to January 2023.

.

Table 1: Time schedule and Gantt chart of the DGMK 844 project

WP	Description	Duration [month]	Start [month]	End [month]
1	Literature Update and Selection of Chemicals	6	1	6
2	Customised Micromodels	9	4	12
3	Core flooding experiments	12	7	18
4	Microfluidic Experiments	12	13	24

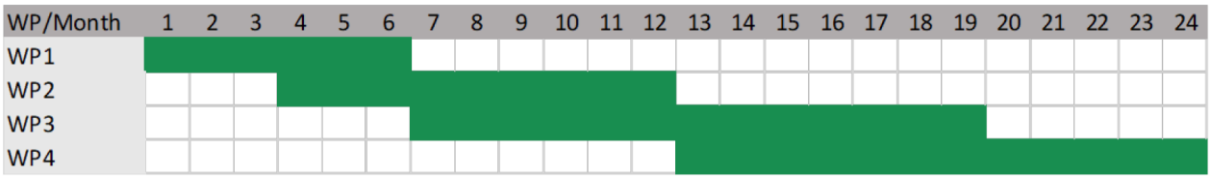

In the first part of the project, the findings on and around conformance control were brought up to date in an intensive literature search. In the second work package, new micromodels were designed and manufactured. These exhibit features in their structure commonly found in reservoirs with degraded conformance. One edition of the models has fractures in its structure, while another has layers of high and low permeability. Various products such as polymers, gels and so-called Relative Permeability Modifiers (RPMs) are used to mitigate conformance problems. Examples of this are used in work packages 3 and 4 both in core floods and in micromodels. Further, the results obtained in DGMK 844 have been published in the course of the project in national conferences. Further, Master, Bachelor and Seminar theses have been performed by ITE students within the research project DGMK 844.

2. Zusammenfassung

In diesem Projekt DGMK 844 wurde die bisherige Forschung zu Conformance Control um die Methode der Mikrofluidik erweitert. Die Dauer des Projektes erstreckte sich über 24 Monate beginnend Anfang Juli 2020. Sie wurde um weitere sieben Monate bis Ende Januar verlängert (Table 2).

Table 2: Time schedule and Gantt chart of the DGMK 844 project

WP	Description	Duration [month]	Start [month]	End [month]
1	Literature Update and Selection of Chemicals	6	1	6
2	Customised Micromodels	9	4	12
3	Core flooding experiments	12	7	18
4	Microfluidic Experiments	12	13	24

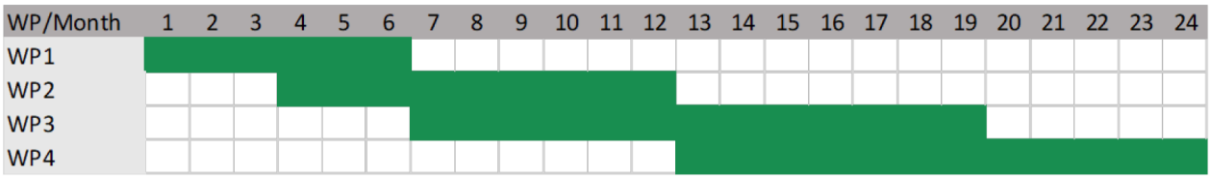

Im ersten Teil des Projektes wurden in einer intensiven Literaturrecherche die Erkenntnisse zu und um Conformance Control auf einen aktuellen Stand gebracht. Im zweiten Arbeitspaket wurden neue Mikromodelle entworfen und hergestellt. Diese weisen in ihrer Struktur Merkmale auf, die häufig in Lagerstätten mit Konformitätseinbußen zu finden sind. So hat eine Auflage der Modelle Risse in ihrer Struktur, während eine andere hoch und niedrig permeable Schichten aufweist. Zur Minderung der Konformitätsprobleme werden verschiedene Produkte wie Polymere, Gele und sogenannte Relative Permeability Modifier (RPMs) eingesetzt. Beispiele hierfür werden in den Arbeitspaketen 3 und 4 sowohl in Kernfluten als auch in Mikromodellen angewendet. Weiterhin wurden die in der DGMK 844 erzielten Ergebnisse im Rahmen des Projekts auf nationalen Tagungen veröffentlicht. Darüber hinaus wurden Master-, Bachelor- und Seminararbeiten von ITE-Studenten im Rahmen des Forschungsprojekts DGMK 844 durchgeführt.

3. Introduction

Conformance control covers a broader range of methods that aim to improve oil recovery and reduce water production of oil fields. Conformance control treatments can help to achieve this through improving the sweep efficiency in the reservoir, which may result in a better macroscopic displacement of the oil. As many reservoirs are heterogeneous, the injected drive water will take the path of least resistance and bypass the oil that is located outside of the high permeability zones. Along the heterogeneity, also the mobility ratio has a high impact on the displacement process. The water production resulting out of the poor sweep efficiency is a problem and a major cost driver during the oil production. By applying conformance control treatments, the flow of the injected water will be diverted to areas of the reservoir that would not been swept by a simple water flood, resulting in a more efficient oil displacement. Due to the better displacement, the water production can be reduced resulting in a reduction of the overall production costs, the oil recovery becomes more profitable, and the lifetime of the field can be ex- tended. Through investing in conformance treatment, the production efficiency and the reserves of a field can be increased.

This research project proposal extents the research efforts analyzing various agents for conformance control undertaken in DGMK 704, utilizing the microfluidic technology established during DGMK 746. Several agents for conformance control or water-shut-off such as in-situ forming gels, microgels or relative permeability modifier are analyzed in microfluidic and core flooding experiments. Therefore, customized micromodels are designed using µCT images of rock material from Bentheimer and Dogger β cores, the same material that is utilized in core flooding experiments. Those micromodels feature common heterogeneities found in reservoirs with conformance control issues resulting in high water cuts.

The duration of this project was scheduled for 30 months starting in July 2020 and ending with the submission of this report in January 2023. This report is structured according to the work packages listed below:

1. Selection of Products and Literature Update
2. Customized Micromodels
3. Core flooding experiments
4. Microfluidic Experiments

4. Methodology

For the experimental part of this work, several different devices and standard working procedures are applied. The setting and operating modes of the used set ups are described in this chapter. This includes the rheology, the micromodels as well as the microfluidic setups for polymer screening and cleaning and the core flooding rig. All used substances and materials are described and their preparation and properties explained.

4.1 Minutes for experimental work from Kick-Off

The project partners agreed on the following parameters for the standard screening experiments in the kick-off meeting from the 7th July 2020:

- Temperature in Bentheimer (BH) sandstone reservoirs ranges between 20 – 100 °C in Dogger β (Dβ) 40 – 50°C. Temperature for all experiments in this phase of the project is set to 45°C.
- Salinity in BH ranges between 100 - 120 g L^{-1} and in Dβ mainly around 80 g L^{-1}. For the experiments it was agreed on the use of a standard brine with a salinity of 100 g L^{-1}.
- A dead oil and synthetic oil with a viscosity of 20 - 30 cP at standard conditions. Oil samples are going to be delivered by Neptune.
- BH and Dβ outcrops to be used for µCT imaging and core floods. Rock material will be delivered by Neptune and/or WintershallDEA.
- Properties of micromodels of BH and Dβ sandstone with homogeneous structure are based on results of rock analysis of the provided outcrops
- Permeability ratio of high and low perm areas in heterogeneous micromodel is set to 1:10.
- The companies which are Halliburton, Poweltec and SNF are going to contribute product recommendations for the above mentioned reservoir properties. From all suggestions, a selection of comparable products will be chosen for bulk analysis to nominate candidates for microfluidic experiments and core flooding.

4.2 Rheology

In Improved Oil Recovery (IOR) and Enhanced Oil Recovery (EOR) applications involving polymers and gels the viscosity of the oil displacing phases is a crucial parameter to evaluate their efficiency. Depending on the mobility ratio *M* of the displacing and the displaced media (see equation 2), the extrusion mechanism are altered. The mobility λ_i is the ratio of the effective permeability k_i of a phase in multiphase flow in porous media and its dynamic viscosity μ_i (see equation 2).

$$M = \frac{\lambda_D}{\lambda_d} \dots (1)$$

$$\lambda_i = \frac{k_i}{\mu_i} \dots (2)$$

Here:

λ_D : mobility of displacing fluid [$m^2.Pa^{-1}.s^{-1}$]

λ_d : mobility of displaced fluid [$m^2.Pa^{-1}.s^{-1}$]

k_i : effective permeability to fluid “i” [m^2]

μ_i : viscosity of fluid “i” [$Pa^{-1}.s^{-1}$]

Wegner shows with microfluidic experiments, that mobility ratios above 1 lead to a loss of displacement efficiency.[1] Polymers for example are utilized in EOR to increase the viscosity of the aqueous phase and to decrease its permeability to obtain more favorable mobility ratios.

The dynamic viscosity is measured with the Kinexus Pro by Malvern under standard conditions at 22°C and 45°C, the latter is the temperature at which the flooding experiments are performed. All unknown substances are analyzed multiple times at both temperatures.

Depending on the properties of the sample, the rheometer offers various geometries as shown in Figure 1. The double gab (DG) geometry (Figure 1a) offers a high contact area between sample and the geometries surface to enable highly sensitive measurements of fluids with very little viscosity, for example water. However, turbulences can occur at very high shear rates. For liquids with low viscosity, but also

for viscoelastic fluids the concentric cylinder (CC) geometry (Figure 1b) can be used. Highly viscous liquids, gels and flexible solids are preferably measured with the parallel plate (PP) geometry (Figure 1c). As default, all samples that are easily pourable are measured with the DG system in this work.

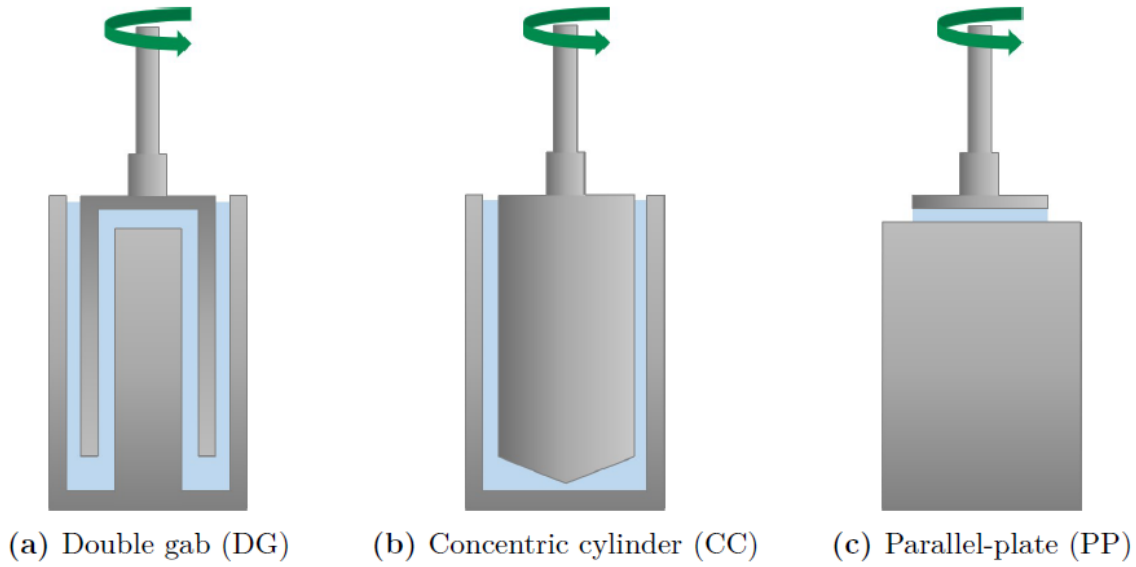

Figure 1: Rheometer geometries

The first measurements will be repeated immediately using the same sample and temperature. Divergent results from the first analysis are an indication for sample degradation due to shear stress. This is relevant for some polymer samples. A subsequent measurement with a new sample of the same substance is needed to confirm the results of the first measurement and to exclude deviations caused by incorrect sampling. Usually the data from multiple measurements is used to calculate a median value. If the data of those individual measurements is analyzed separately, they are labelled as follows: the first number represents the sample of the measured substance and the second number counts the number of measurements taken with this sample. For example, the label “X 1.2” identifies the data as the results from the second measurement of the first sample of substance X. The shear rate is varied between 0.1 and 1000 s^{-1} with ten measurements per decade if not stated differently.

4.3 Fluids

In this project, products to tackle conformance control issues are analyzed and applied in comparable flooding experiments. Those experiments are conducted under reservoir conditions with a thinned dead oil and a brine with a salinity of 100 g L^{-1}. Their preparation and properties are given here.

4.3.1 Oil

The used oil is a dead oil from the well Ringe 6 delivered by Neptune Energy. It is a black, semi-solid mass, whose viscosity is measured at various temperatures and alternatively to the standard procedure with a concentric cylinder system due to the high viscosity of the sample (Figure 2 and Table 3). The oil is thinned with n-decane to match the targeted viscosity of 20 to 30 mPa.s^{-1} at standard conditions (Figure 3 and Table 4) and filtered. Its final properties are given in Figure 4 and Table 5. μ_{10} and μ_{100} are the viscosities at shear rates of 10 and 100 s^{-1} respectively.

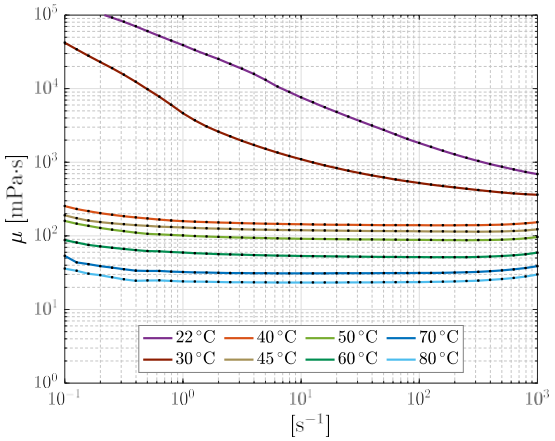

Figure 2: Dead oil at different temperatures

Table 3: Viscosity of dead oil at different temperatures

T [°C]	μ_{10} [mPa s]	μ_{100} [mPa s]
22 °C	7640	1943
30 °C	1101	524.5
40 °C	144.4	140.1
45 °C	119.6	116.0
50 °C	91.85	88.61
60 °C	53.36	51.50
70 °C	31.02	31.36
80 °C	23.35	23.68

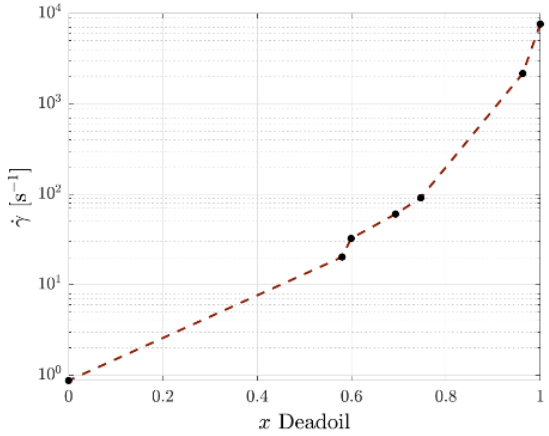

Figure 3: Viscosity of dead oil thinned with n-decane at different proportions

Table 4: Viscosity of dead oil thinned with n-decane at different proportions at room temperature

x [-]	μ_{10} [mPa s]	μ_{100} [mPa s]
1.00	7640	1943
0.96	2166	1156
0.75	91.59	76.24
0.69	60.48	52.16
0.60	32.52	30.06
0.58	20.26	18.77
0.00	0.8721	0.8829

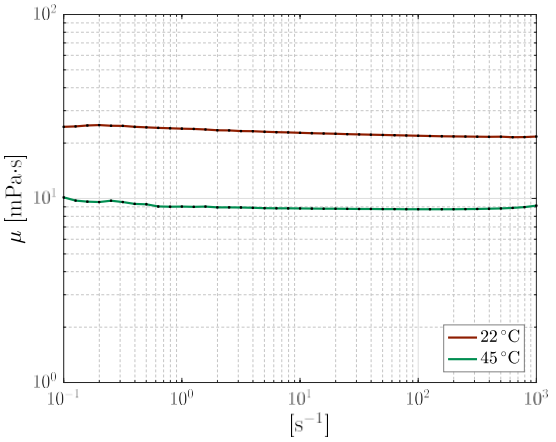

Figure 4: Viscosity of dead oil thinned dead oil

Table 5: Viscosity of dead oil

T [°C]	μ_{10} [mPa s]	μ_{100} [mPa s]
22	22.77	21.96
45	8.845	8.768

4.3.2 Brine

The brine is a solution of sodium, potassium, calcium, magnesium, chloride and sulphate. Its composition is similar to seawater (scientific subsea water) with an overall salinity of 100 g L−1. The used salts and their quantities are listed in Table 6. For the preparation of the brine, the salts listed in Table 6 are weigh in into a volumetric flask, which is then filled to the calibration mark with distilled water. The solution is filtered under nitrogen atmosphere through a 1.2 µm filter into a clean bottle. Furthermore, for polymer preparation, the solution is degassed in vacuum and saturated with nitrogen to minimize its oxygen content. The pH value of the brine at 25°C is 7.15.

Table 6: Brine composition

Salt	***c*** **[g L^{-1}]**
NaCl	57.5
KCl	2.0
$CaCl_2$	3.0
$MgCl_2 \cdot 6\,H_2O$	27.5
Na_2SO_4	10.0

4.3.3 Other aqueous salt solutions

The preparation of some of the conformance control agents requires for different brines such as a 2 wt.% KCl or a 6 wt% NaCl solution. All these solutions are prepared like the brine in the previous Section 4.3.2. For each percent of the targeted solution, 10 g of the salt is weigh in into a 1 L volumetric flask. The flask is filled with distilled water to the calibrated mark. After the salt is fully dissolved, the brine is filtered under nitrogen atmosphere through a 1.2 µm filter into a clean bottle.

4.4 Rock samples

Four pieces of a Bentheimer (BH) core are delivered by Neptune Energy (Figure 5a) and four Dogger *β* (Dβ) cores by Wintershall Dea for core flooding (Figure 5b).

4.4.1 Bentheimer

As can be seen in Figure 6, several small cores with a length of 60 mm and diameters of 10 mm for µCT-imaging and 30 mm for core flooding are drilled from the provided cores (Figure 5a). The rock material is unconsolidated and only a fraction of the drillings are successful. They are labelled according to the source material either with BH for Bentheimer or D*β* for Dogger *β* sandstone followed by the number of the core and the number of the bore hole of their small cores.

(a) BH (b) Dβ

Figure 5: Provided core material

Figure 6: Provided BH cores after drilling of small cores

Core cleaning

All cores need to be cleaned for the routine rock analysis, µCT-imaging and flooding experiments. A core is considered clean when the extract remains colorless and clear. Afterwards the rock material should feature water-wet properties. Several different methods for core cleaning are described in literature: distillation/extraction in a Dean-Stark or Soxhlet apparatus, flow-through core cleaning, centrifuge flushing, gas-driven solvent extraction, and supercritical fluid extraction and critical point drying. From all of these methods, the extraction is the most gentle procedure. However, the solvents might not penetrate the center of the core, leaving areas soiled. A more effective method would be the flow-through cleaning, where the core is placed in a holder and the solvents are injected from one front end to the other.[2] However, mounting the core into the holder puts the core under mechanical stress and increasing its risk of breaking.

At first, the two intact cores BH-3-5 and BH-3-7 as well as the smaller pieces of the BH-3-4 drilling (all samples with a diameter of 10 mm) are placed in a Soxhlet apparatus as shown in Figure 7 and Figure 8.

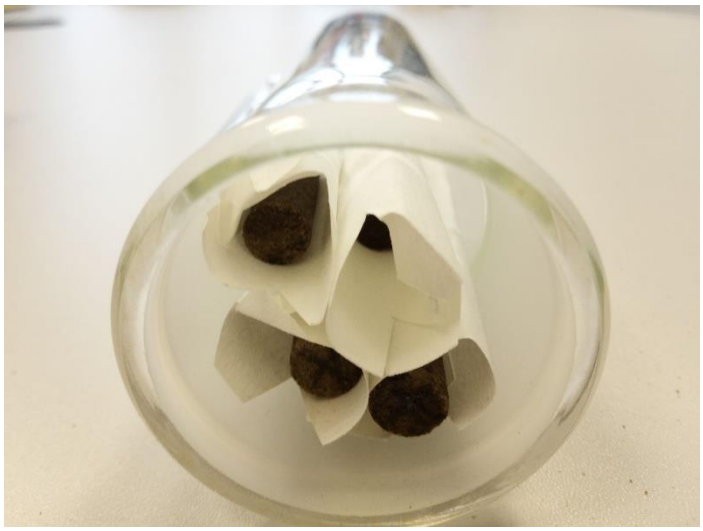

Figure 7: BH cores for µCT-imaging in Soxhlet top piece

Figure 8: Soxhlet apparatus

The extraction starts with toluene as solvent. Toluene will dissolve any organic remains in the pores and on the rock surfaces. In the Soxhlet apparatus, the solvent is distilled, condensed and dropped into the extractor where the cores soak in the hot extract, which is periodically siphoned off to be replaced slowly by freshly distilled solvent. After 24 hours, the extract remains colorless, but the extraction is continued until 48 hours. The toluene is replaced for methanol to dissolve salts and other water-soluble precipitations and the extraction is continued for another 48 hours. This procedure is repeated 2 times (48 hours toluene followed by 48 hours methanol) to ensure the rock sample is clean. At the end of the extraction, the cores are removed and dried first at room temperature, then in a ventilated oven at 50°C. While the core BH-3-5 remained intact, BH-3-7 fell apart during extraction.

The cleaning of the cores with the larger diameter of 30 mm was planned to be performed with the flow-through method. Given that even the gentle extraction let to a disintegration of the rock material, the cores BH-2-3, BH-3-1 and BH-4-1 are cleaned by immersion in the different solvents for periods of three days with daily exchange of the extract for fresh solvent, again starting with toluene. BH-3-1 and BH-4-1 already showed several fractures beforehand, BH-3-1 fell apart after the first 24 hours immersed in methanol. The cleaning of other cores in a Hassler Cell using the flow-through approach left the cores also unconsolidated plugging the set up. In agreement with the project partners, it was decided to switch to a Bentheimer outcrop available at the ITE instead for all upcoming experiments.

4.4.2 Dogger ß

Wintershall DEA provided four small cores drilled from Dogger *β* core material.

Core cleaning

The provided cores were cleaned by Wintershall DEA by alternate immersion in toluene and methanol, CT scanned and shipped to the TU Clausthal for further experiments.

5. Work Package – 1 Selection of Products and Literature Update

5.1 Literature Update

Conformance Control is an important method to help reduce the amount of produced water and consequently operating costs, while at the same time increasing oil production rates, reserves, and asset value. Continuous research and application of the latest technologies provide the basis for expanding the application into even more complex reservoir conditions. The industry interest in research, innovative designs and application procedures for Conformance Control continues to grow as the increasing numbers of publications in this area every year indicates (see Figure 9).

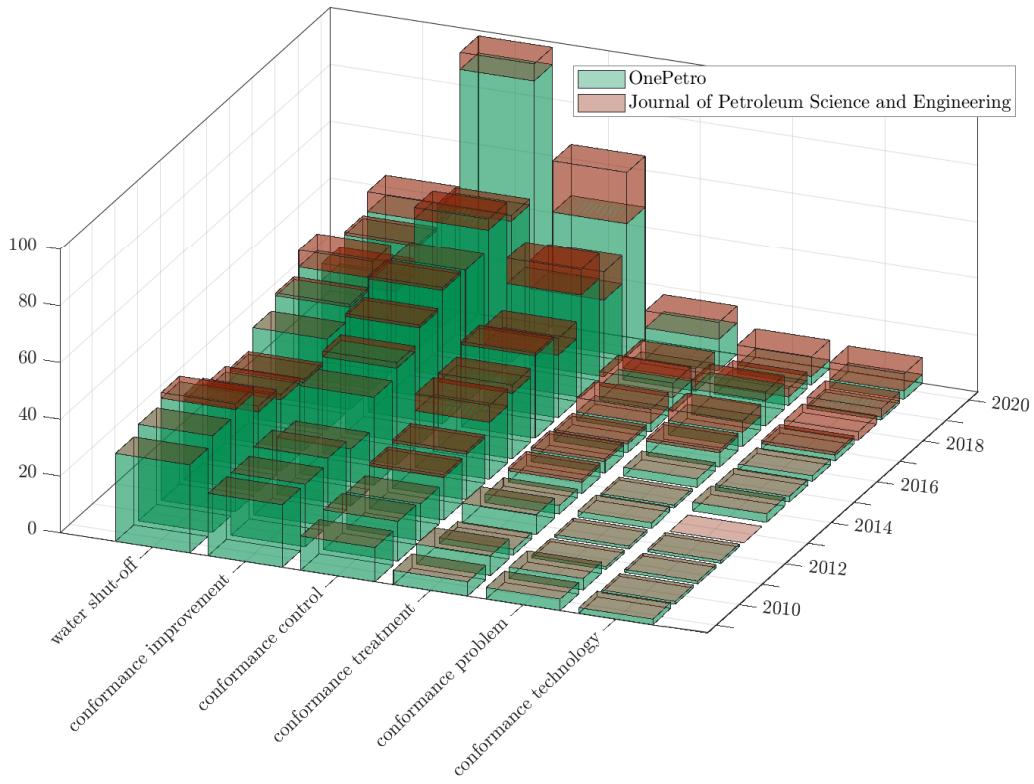

Figure 9: Number of publications linked to specific keywords over time

This literature review was performed within the scope of the ongoing DGMK project

844 and is constitutes an addendum to the 2009 DGMK Report 704-1, an industry funded review of the status of Conformance Control. The development of new types of polymers and polymer-gels, as well as the improvement of existing formulas by combing them with nanoparticles, microorganisms, and other materials have been main topics in publications after 2009.

As important as the reduction of water production and relative increase in oil production is the reduction of the environmental impact of the applied chemicals. In many countries, regulatory requirements are becoming more stringent as today's society becomes more sensible to the long-term effects of its acts on our planet. Hence, the research now also targets the adherence to even more stringent environmental controls, as this is fundamental for the license to operate. In this regard, it is necessary to reduce harmful chemicals in the polymer solutions, or completely replace those by more environmentally friendly alternatives. The other research focus is on higher resistance of agents regarding the range of pH, salinity, and temperature. Higher stability of those polymers and polymer systems is a key enabler for application in more complex reservoirs. Many papers evaluate the effectiveness of new biopolymers and new types of microorganisms and offer promising results.

This overview will highlight which chemicals, components and combinations are favored to improve desired effectiveness and a wider application range. Notably the effect of nanoparticles, recrosslinkable preformed particle gels (RPPG) and gels suitable for CO_2 application to address conformance control for miscible EOR treatments in reservoirs will be discussed, as will the more environmentally friendly design, organic cross-linkers for gel formation and new types of microorganisms. Those research topics are touched upon, and future trends identified.

5.1.1 Improvement of Stability

The improvement of the stability of polymers and microgels especially towards high salinities, high temperatures and low pH values, is relevant to apply conformance treatments with synthetic and biological polymers to more complex reservoirs. Biopolymers in general already have a higher stability against temperature and shear degradation than synthetic polymers. This also includes the gel strength of the polymer gels after placement in the reservoir.[3] Especially high temperatures which can often occur in the reservoir are a challenge for synthetic polymers like polyacrylamide (PAM) and synthetic polymer gels.[4–6] Biopolymers like Xanthan Gum and Schizophyllan have a higher resistance and can be applied to harsher reservoir conditions.[5,7] Schizophyllan shows short-term stability up to 135 °C and long-term stability up to 96 °C in laboratory tests. Scleroglucan, another biopolymer, shows temperature

resistance up to 130 °C. In general biopolymers can be applied up to temperatures of 70 to 90 °C. The reason for the high resistance is the high molecular weight and the structure of the biopolymers which makes them less sensitive to high reservoir temperatures, hardness, and salinities.[5] Conventional PAM has only a single strain structure while Xanthan Gum has a double helix structure. Schizophyllan and Scleroglucan have even a triple helix structure which makes them more stable against physical and chemical degradation.[6] The resistance against high salinity environments was validated in a field test at the Bockstedt oil field in 2012.[8]

Another stability improvement was achieved by combining polymer and polymer gels with nanoparticles. Nanoparticles gained interest for a long time as they can increase the stability and the viscosity of emulsions.[9] Due to the strive for less environmental impacts, biological nanoparticles are interesting again. Especially cellulose nanocrystals (CNC´s) have been in the focus as a biological alternative. This alternative showed a high potential to block of flow channels and even acts as a relative permeability modifier (RPM) during laboratory tests. In general, nanoparticles have a good chemical and physical stability making them interesting for conformance control treatments in reservoirs with harsh conditions. Additionally, many nanoparticles have little impact on the environment.[9] The physical and chemical improvement through nanoparticles was verified in different studies. In one study, silicon dioxide nanoparticles and aluminum oxide nanoparticles have been added to the Xanthan Gum biopolymer. The gel then used for the test was created by applying chromium (III) as a cross-linker. During the experiment, the gelation time and the gel strength have been evaluated. It could be conducted that none of the two nanoparticle types had a significant impact on the gelation time, but they increased the gel strength through an improved physical bonding. A concentration of 5000 ppm of nanoparticles were enough to achieve a higher gel strength of the polymer gel. Comparing the two used nanoparticle types it was identified that the gel strength improvement with aluminum oxide nanoparticles was better than with silicon dioxide nanoparticles.[10]

Next to this, also the effect of nanosilica on the polyacrylamide tert-butyle acrylate (PAtBA) was investigated, which was already successfully applied in the field. The development of this polymer was especially mentioned in the 2009 DGMK Report 704-1. Two different cross-linkers have been used in the gel design: the organic cross-linker polyethyleneimine (PEI) and the inorganic cross-linker chro- mium (III) acetate (CrAc3). The aim was to use nanosilica alongside CrAc3 and PEI cross-linkers to strength the gel and improve its stability as a water shut-off treatment. In laboratory experiments the effect of nanosilica on the gel strength could be verified. Both cross-linkers resulted in a very stable and temperature resistant gel and both combinations of PAtBA with the organic and with the inorganic cross-linker showed a significant

increase in strength through adding nanosilica. The storage modulus of the gel with PEI as a cross-linker increased by 127% while the storage modulus for the gel with CrAc3 increased by 51%. Therefore, the strong stability improvement effect of nanosilica on different polymer gels was verified, whereby the improvement effect on gel with the organic cross-linker was higher than with the inorganic cross-linker. The improvement of PAtBA/PEI with nanosilica resulted in a gel that can resist temperatures up to 160 °C. Before PAtBA/PEI was already successfully field tested in reservoirs with a temperature of 70 to130 °C.[11]

The field application of nanoparticles has been confirmed in various pilot tests. In the Algyo field in Hungary the trial with a combination of silicates, polymers and nanosilica was very positive. The water cut could be decreased from 95-98% down to 40% on average. Due to the availability of all components in a liquid form also the mixing the preparation for the injection was easier and cheaper and due to the components also more environmentally friendly.[12] Another field test with nanoparticles was conducted in 2020/2021 in Columbia where a Brightwater solution was injected into a mature field with temperatures up to 60 °C and salinities above 30000 ppm resulting in a decrease of water production and an increase in recovery. It is stated that the used solution is even applicable up to 150 °C and due to the promising results, the treatment is planned to continue in 2022 and 2023.[13] At the Changqing oil field in China in 2021 a test with nanospheres which are less affected by temperature and salinity was conducted. The salinity of the field is 8800 mg/L, and the temperature is up to 130 °C. Despite these harsh conditions the conformance treatment showed promising results.[14]

Among the stability, improvement effect of the application of biopolymers one organic cross-linker that especially showed promising results is the OC-3 system that in combination with a terpolymer created an in-situ polymer gel that has high resistance against temperature. The gelation time as well as the gel strength of this polymer gel can be controlled by changing the concentration of the components. The polymer gel showed a strong resistance against temperatures up to 149 °C.[4]

Another development that emerged in the recent years is targeting the stability of polymers during the injection into the reservoir. During the injection process polymer-chains can be damaged or even break caused by the friction inside of the valves. The damage during the injection often happens in offshore fields where more valves are placed on the seabed. To avoid damage two different approaches can be used. Either the valve can be changed into a “polymer friendly valve” or the polymer-chains have to be protected during the injection. Because changing the valves is a very complicated procedure, the modification of the injected polymers is usually the better option. To

protect the polymer-chains during the injection their resistance against shear must be improved. If the shear stability of the polymer just have to be increased slightly, because the shear rate in the valve is not extreme, ATBS monomers can be added to the solution. If increasing the resistance of the polymer is not enough to protect it, the usage of delayed viscosity polymers (DVP) can be the key to avoid damage. The delayed viscosity polymers are inverse emulsion products containing acrylamide copolymers inside of a shell. During the injection, the polymers are inside of a shell and are protected against shear degradation from the valves. With time or with temperature increase in the reservoir, the shell will break up and releases the polymers resulting in an increase in viscosity and a polymer solution is created. The technique was just developed recently and has not been tested in the field yet.[15]

Other developments also have been made toward preformed particle gels (PPG´s) which showed their advantages in conformance control in thousands of wells over many years.[16,17] Besides these advantages it was identified that PPG´s are not able to block of very high permeability fractures and channels due to their limited particle size. To address this, a new recrosslinkable preformed particle gel (RPPG) has been developed. This polymer gel consists of larger particles but can still swell inside the reservoir after placement in the fractures. This RPPG combines the advantages of preformed gels and in-situ cross-linkers. Laboratory tests performed on the RPPG showed that its swelling could be controlled from tens of nanometers to a few millimeters by the amount of water, the salt concentration and the temperature. The polymer gel showed a high stability with an elastic gel modulus from 300 to 10800 Pa, lasting for more than six month in a temperature range from 23 to 80 °C. Due to the abilities the RPPG is very promising for conformance treatments for high permeability fractures.[17] A field test with delayed swelling preformed particle gel started in 2016 at the HD oil field by PetroChina demonstrated the promising results while still ongoing as the injected solution was valid for more than 36 month in reservoir conditions of about 110 °C and a salinity of close to 3000 g/l.[18]

A new idea for the improvement of conformance control also emerged for the in-situ control of the polymer gel swelling. Hereby tests with hydrochloric acid (HCL) have been conducted in the laboratory. It was observed that the gel swelling decreased with increasing brine and acid concentration (decreasing pH) and at the same time the gel strength increased. To remove gel from low permeability zones where gel swelling was unwanted, HCL can be applied resulting in a recovery of on average of 95% of the original permeability.[19]

Another development has been made regarding the application of CO_2 injection. The aim was to develop a PPG that can improve the sweep efficiency, especially in CO_2-

EOR treatments. The need for this development is caused by the dehydration that many synthetic gels like HPAM or PSAP (polyacrylamide based superabsorbent polymer) face upon contact with CO_2 resulting in a decrease of stability and plugging efficiency. This decrease often yields to a water or gas breakthrough. To prevent dehydration of polymer gels different novel particle based gels have been developed including AMPS-based PPG´s, CO_2 responsive PPG´s (CR-PPG) and CO_2 resistance PPG´s (CRG).[20] The particle size of these polymer gels can be controlled and the range can be adjusted from millimeters down to nanometers. Milimeter seized particles are used for fracture and near wellbore treatments while the micro and nanometer seized particles are used for far wellbore treatments.[21]

Along CRG also AMPS has a high resistance against CO_2 and its swelling can be controlled by combining it with cross-linkers. Laboratory tests have shown a strong increase in plugging capability of the APMS-based particle gel compared to PSAP.[20] The hydrogel, that is based on hydrophobically modified CO_2-sensitive moieties has been studied further.[22] This CO_2-responsive preformed particle gel (CR-PPG) has the specific capability to swell further upon contact with CO_2 in a water environment resulting in a better blocking of the high permeability channels.[20, 22] Laboratory tests identified that the CR-PPG can swell several times of its original volume upon contact with a water-CO_2-mixture. By using different temperatures and salinities, further characteristics of the gel could be determined. It was identified that the swelling depends on the CO_2 and the salinity, but does not depend on the temperature. An increase in the CO_2 amount yielded in a stronger swelling of the gel while an increase in natrium cloride concentration (NaCl) resulted in a decrease of the swelling. Additionally, a good stability with almost no reduction in shear strength was verified over six month at a temperature of 40 °C.[22] Besides the improvement of the stability in a CO_2 environment the novel particle based gels are more environmentally friendly compared with other synthetic polymer gels.[20] The research towards these gels is support by the goal of the energy industry to become carbon neutral.

The global reduction in CO_2-emissions was manifested in the Paris-Agreement (2015) and has a high impact on the energy industry. The emissions of CO_2 along the oil production are a one of the main areas of interest for every energy company nowadays. The charges for the emissions of CO_2 are a cost factor in every operation and their impact on the economics of projects are likely to increase further. To reduce CO_2 emissions, carbon capturing and storage (CCS) and CO_2-injection gained a high level of interest in the industry.[20] With the injection of CO_2 new challenges are occurring for the stability of conventional polymers and polymer gels as well as for biopolymer due to the acidizing behavior of CO_2. Along the improvement of the fluids used in conformance control there also have been developments on gases and foams. The

research for foam improvement focused on CO_2 because it is expected that the usage of as CO_2 EOR method will increase in the future. To improve the stability of CO_2 foam and reduce the mobility ratio, nanocellulose fibril (NCF) were added. The mixture of CO_2 and NCF´s then resulted in denser and thicker bubbles, which improved the stability of the foam by reducing liquid drainage, bubble coalscene as well as the effect of high temperature and crude oil on the foam. Conducted laboratory tests with the NCSCO_2-foam showed promising results by delaying the gas breakthrough and increasing the oil recovery by 8.6% OOIP (original oil in place).[23]

5.1.2 Reduction of Environmental Impact

One of the trends identified in the 2009 DGMK Report 704-1 on development of conformance control treatments is conducted towards the impact, which the used polymers and polymer gels have on the environment. For a reduction of the impact, research has been carried out to either improve the existing polymers and polymer gels by reducing the amount of environmental harmful chemicals or to replace them completely with less harmful alternatives. The focus of the industry and the research institutions for addressing this challenge is hereby on less harmful cross-linkers, new types of organic cross-linkers, biopolymers and microorganisms. These alternatives have been already known for a long time, but they just gained interest again in the recent years due to stricter conditions for applying chemicals like the existing cross-linkers, polymers and polymer gels in the field.[7,24] As the restrictions are increasing the usage of more environmentally friendly polymers in conformance control treatments is required.

One more environmentally friendly alternative for replacing heavy metals containing cross-linkers like Cr-III is sodium silicate, also known as water glass. Sodium silicate has only minor effects on the environment and besides shows high resistance against temperature, an adjustable gelation time and a high viscosity development in combination with biopolymers making it even more interesting for field applications in extreme reservoir conditions.[25] Due to the adjustable gelation time, it enables conformance treatments deep inside the formation, whereby the gelation time and activation of the sodium silicate is controlled through the design of the solution tailored according to the subsurface conditions like pH value and salinity.[3] Due to the advantages of silicates and the development of nanotechnology, nowadays nanosilica receives more attention as an environmentally friendly alternative for further stability improvement. The nanosilica will be discussed in the next chapter due to their strong influence on the stability of the polymer gels.

Besides nanosilica, organic cross-linkers are nowadays a widely used alternative to replace inorganic cross-linkers. Organic cross-linkers like polyethyleneimine (PEI) are based on carbon chains that have almost no impacts on the environment. Very promising as a cross-linker is thereby an OC-3 system, that in combination with a polymer showed even high resistance against temperature up to 149 °C.[4]

Biopolymers are another alternative. They are mainly used to replace the existing synthetic polymers that are typically based on polyacrylamide and can there- fore be harmful for the environment.[7] The lesser impact on the environment is due to the base of biopolymers. The biopolymers consist of polysaccharides instead of polyacrylamides. Polysaccharides consist of components growing naturally while polyacrylamides are synthetic. One of the most used polysaccharides is Xanthan, also referred to as Xanthan Gum.[5,7] Other known biopolymers are Schizophyllan and Scleroglucan. Especially Schizophyllan showed already promising results in a field test in Bockstedt in Germany in 2012.[8]

Along with the lesser impact on the environment, biopolymers have another interesting characteristic. They are often more stable in high salinities and high temperatures where synthetic polymers reach their limitations first.[4,5,7] Additionally, biopolymers are usually less affected by shear degradation and adsorption.[26] If used as a viscosifier, they can increase the viscosity of the injected fluid sometimes stronger than conventional polyacrylamides.[16] Biopolymers also come with a disadvantage compared to conventional polymers. They are highly affected by bacterial attack and have a higher biodegradability than polyacrylamides.[5–7,26] The biological degradation especially occurs in the near wellbore area and depends on several different factors: physical characteristics of the reservoir, the stability of the biopolymer regarding temperature, salinity and pH-value, and the cell number of the biopolymer.[7] Their sensitivity to biodegradability can be reduced by adding microbial inhibitors like bio acids, but this conditioning must be performed with caution as a wrong amount of bio-acids can yield to a negative impact. To avoid a negative effect, it is important to examine the field data, besides fluids from the reservoir and injected fluids, also mineralogy for geomechanical characteristics. It is recommended to collect as much information as possible to carefully select the right biopolymer for the conformance control treatment.[7,26] Next to the technical challenges for the application of biopolymers, also the economics must be considered. Comparing the costs for Xanthan Gum with hydrolyzed polyacrylamide (HPAM) biopolymers often require more expenditures than synthetic polymers.[26]

Besides using biopolymers instead of conventional polymers for conformance control, replacing polymer gels by microorganisms is another alternative more environmentally

friendly option. The application of these organisms in conformance control treatments to improve the recovery is promising with almost no impact on the environment. An additional benefit is that conformance treatments with microorganisms are cost efficient.[24, 27] As conformance treatment they can have several effects: producing biomass causing bio clogging, redirecting the fluid flow, producing gas in situ, and changing the wettability of the rock surface.[27] The lower environmental impact and the stated useful additional effects compared to polymer gels resulted in a high interest and an increase in research towards microorganisms. Like with the gel treatments for conformance control there are still uncertainties about the exact behavior of the microorganisms inside of the reservoir and how their placement and growth can be accurately predicted to avoid negative impacts on the recovery from the reservoir. Moreover, the stability, the behavior, and the growth of the microorganisms under different conditions including temperature, salinities and pH must be evaluated to increase the application range of microorganisms as a conformance treatment. One main area of interest in the upcoming years will be the understanding of the effect of the biomass on the relative permeability by changing the wettability of the grain surface. The process has still not been fully understood and since it can have a large impact on the conformance, it is an important task to continue research on this topic to increase the knowledge of the process. By understanding the wettability changes the conformance treatment with microorganisms can be improved further and thus the oil-recovery and the economics of oil fields can benefit in the future.[7,24,27]

5.1.3 Future Trends

The strive to develop less environmental harmful chemicals for conformance control will continue as more restrictions and laws demand respect for the environment and safe-being of people. Improving existing polymers by applying new types of cross-linkers and nanoparticles or replacing them entirely by biopolymers or microorganisms is the trend of the future. The research is likely to continue to focus on biopolymers and microorganisms and probably even increase in the next years. In addition, the improvement of the application range of already existing polymers is expected to continue through the development of new cross-linkers and by using nanotechnologies to combine polymers with different nanoparticles. There is a high need for stability improvement to apply conformance treatments in more complex reservoirs as many of the simple fields are already at the end of their lifetime and the largest potential for additional oil recovery lies in complex reservoirs. This direction is supported by rising oil prices, which will allow an increase of research and the number of field trials. For selecting the proper conformance treatment, a precious determination of the root cause of the conformance problem is necessary. It is likely to be seen that artificial intelligence (AI) will be applied for a better and more precise identification of the root

cause. Furthermore, an improvement in computational chemistry and better simulation technologies will assist in the identification of the most effective conformance treatment as well as with the adjustment of the used polymers. Based on the number of publications in the recent years as well as interviews with industry representatives it can be expected that conformance control will remain a key topic in the future for the energy industry.

5.2 Investigated Products – Properties, Application and Working Mechanisms

5.2.1 H_2Zero™

The commercially available product H_2Zero™ by Halliburton is based on polyacrylamide *tert*-butyl acrylate (PAtBA), which is cross-linked with polyethylenimine (PEI) to form the temperature resistant gel.[28]

Product description

Halliburton provided two samples to prepare H_2Zero™; the polymer HZ-30 and the cross-linker HZ-20. Both are clear, colorless and highly viscous liquids. Following information for preparation and application are given by the manufacturer:

- Quantities for 1 L:

730 mL	tab water*
14.9 g	KCl
250 mL	HZ-30 polymer
20 mL	HZ-20 cross-linker

- Preparation:

1. Fill the tap water* into an appropriate container.
2. Dissolve the potassium chloride in the water.
3. Add the polymer HZ-30 to the brine under stirring with a magnetic stirrer or

a similar device. Using a high-shear blender is not recommended, because it could generate foam.

4. Add the cross-linker HZ-20 to the polymer solution and keep mixing until a homogeneous solution is obtained, which should take only a few minutes.

- Application:
  1. Remove 50 to 100 mL of the H_2Zero™ to check the gel time and use the remainder for the core test.
  2. Determine the core permeability to brine as deemed appropriate for the particular test.
  3. For the treatment of the core, injection of 10 PV H_2Zero™ with a rate of 1 - 5 mLmin^{-1} is recommended.
  4. Place the small H_2Zero™ sample taken earlier into a water bath at test temperature. Check the sample periodically for gelation. After ≈ 4 h a rigid, non-movable gel should have formed.
  5. Shut in of the core for at least 24 hours.
  6. Determine the final permeability. This is done by raising the pump pressure in 100 psi (6.89 bar) increments with a minimum holding time of 10 minutes at each pressure. As soon as flow is observed, the final permeability can be measured.

* To ensure reliable and reproducible results, the tab water will be replaced by distilled water as it is used for the preparation of every aqueous solution in this work.

Rheological analysis

Before H_2Zero™ is prepared, its reactants are analyzed. The results are given in Figure 10 and Table 7.

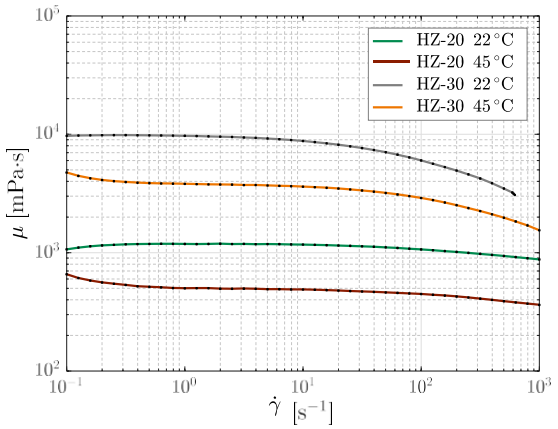

Figure 10: Viscosity of H2Zero™ reactants

Table 7: Viscosity of H2Zero™ reactants

Sample	T [°C]	μ_{10} [mPa.s]	μ_{100} [mPa.s]
HZ-20	22	1170	1065
HZ-20	45	489	447
HZ-30	22	8783	6011
HZ-30	45	6139	2886

A small sample of H2Zero™ for rheological characterization only is prepared by adding 1.485 g potassium chloride (KCl) and 25 mL HZ-30 to 72.956 g of distilled water following the instructions listed above. As soon as 2 mL HZ-20 are added to the mixture, a small sample is transferred to a small bottle for gel check and the rest to a larger container for sampling in regular periods. Both beverages are stored in a water bath at 45 °C. Every hour a sample is taken for analysis (Figure 11 and Table 8) and gel checking (Table 9).

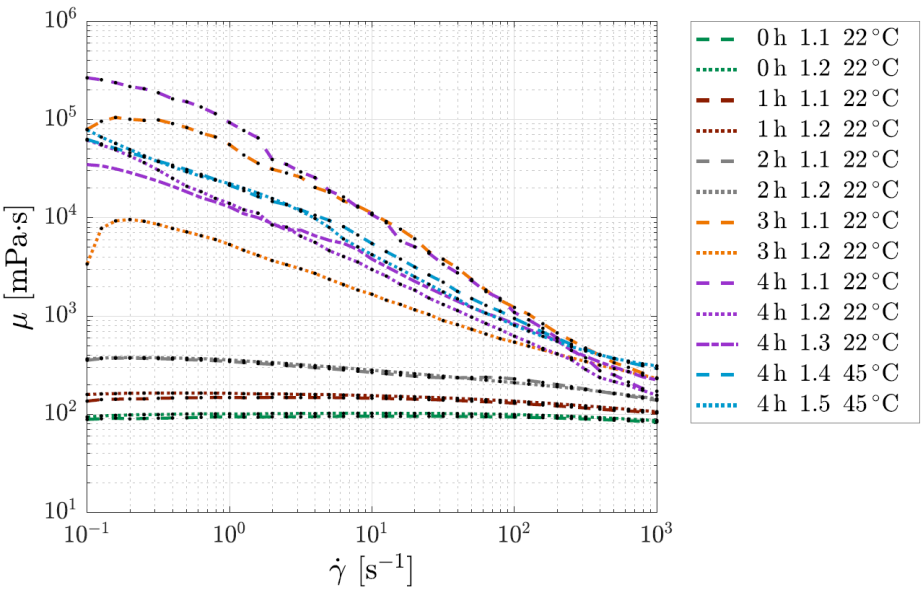

Figure 11: Viscosity alteration of H_2Zero™ during gelation – Part

Table 8: Viscosity of H2Zero™ during gelation – Part I

t_g [h]	No.	T [°C]	μ_{10} [mPa s]	μ_{100} [mPa s]
0	1.1	22	94.84	93.57
0	1.2	22	101.9	99.07
1	1.1	22	145.2	129.3
1	1.2	22	154.2	135.5
2	1.1	22	265.7	228.5
2	1.2	22	280.4	209.1
3	1.1	22	11 130	1221
3	1.2	22	1662	540.7
4	1.1	22	10 740	1085
4	1.2	22	2965	621.6
4	1.3	22	3784	830.5
4	1.4	45	5466	942.9
4	1.5	45	4207	802.9

Table 9: Gel strength of H_2Zero™

t_g [h]	Gel strength
0	A
1	A
2	B
3	B – C
4	E
5	G
6	H
7	I

During the first two hours of gelation, the viscosity increases gradually. The direct repetition of the measurement using the same sample shows no significant alteration of the sample. This changes rapidly after three hours; the viscosity of the first analysis of a sample is immoderately increased to the subsequent measurements using the same sample. It has to be mentioned that the geometry for rheological analysis had to be switched from the double gap to the concentric cylinder geometry. To observe if the gel disintegrates, the sample (after gelation for four hours) is measured twice at room temperature. The viscosity does not change after the second measurement. It is concluded that the shear stress of the first measurement breaks down entangled polymer strains and loose inter-cross-linkages. Therefore, this sample should either be pre-sheared for reliable analysis or it needs to be differed between a pre-sheared and a non pre-sheared sample.

The viscosity of the sample taken after four hours of gelation is measured a forth and a fifth time at 45 °C. Here, the viscosity is higher than during the measurements at room temperature. This observation is most likely caused by the ongoing gelation as shown in Table 9. By the time of these measurements, five hours have passed since the preparation of the H2Zero™. To exclude any errors occurring due to the change of the analysis setting, this gelation experiment is repeated with the concentric cylinder geometry for all measurements. Figure 12 shows all results. The results reveal on one hand that the reaction rate increased after two hours and that from this point onward the viscosities of non- sheared and sheared samples differ significantly on the other. Therefore, Figure 13 sorely shows the pre-sheared results. Both test series reveal a gelation time between four and five hours at 45 °C with ongoing consolidation after this time range.

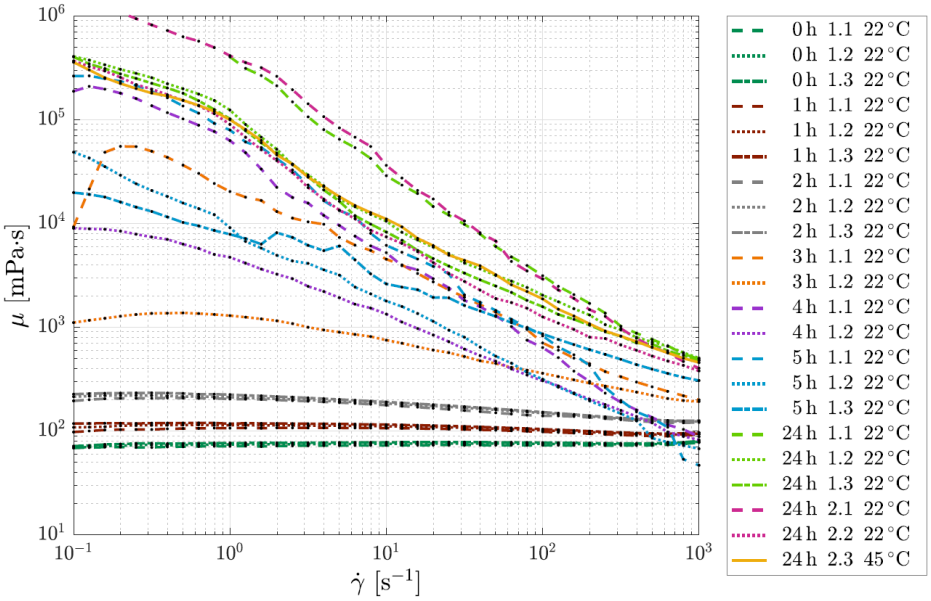

Figure 12: Viscosity alteration of H_2Zero™ during gelation – Part II

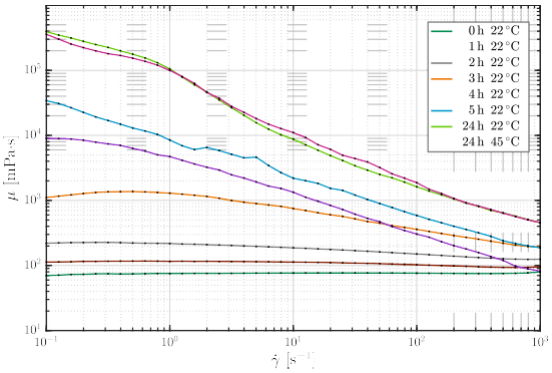

Figure 13: Viscosity alteration of H2Zero™ during gelation (pre-sheared samples)

Table 10: Viscosity alteration of H2Zero™ during gelation – Part II

t [h]	T [°C]	μ_{10} [mPa s]	μ_{100} [mPa s]
0	22	76.60	76.23
1	22	113.1	102.9
2	22	187.1	150.3
3	22	750.4	359.8
4	22	1338	304.4
5	22	2200	588.3
24	22	8731	1623
24	45	11 030	1873

5.2.2 FormSeal

FormSeal by Halliburton is a temperature activated cross-linking polymer gel.[29]

Product description

Halliburton provided three liters of Gascon 469 to prepare FormSeal. It is a slightly turbid, colorless and low viscous liquid. Following information for preparation and application are given by the manufacturer:

- Quantities for 1 L:

  870 mL GasCon 469

  130 mL 6 $_{wt}$% sodium chloride (NaCl) solution

- Preparation:

  1. Fill the GasCon 469 into an appropriate container.
  2. Add the 6 $_{wt}$% NaCl solution and mix until a homogeneous solution is obtained.

- Application:

  1. Remove 50 to 100 mL of the FormSeal to check the gel time and use the remainder for the core test.
  2. Determine the core permeability to brine as deemed appropriate for the particular test.
  3. For the treatment of the core, injection of 10 PV FormSeal with a rate of 1 - 5 mL min^{-1} is recommended.
  4. Place the small FormSeal sample taken earlier into a water bath at test temperature. Check the sample periodically for gelation. After ≈5 h a rigid, non-movable gel should have formed.
  5. Shut in of the core for at least 24 hours.
  6. Determine the final permeability. This is done by raising the pump pressure in 100 psi (6.89 bar) increments with a minimum holding time of 10 minutes at each pressure. As soon as flow is observed, the final permeability can be measured.

Rheological analysis

At first, the delivered agent Gascon 469 is analyzed. The results are given in Figure 14 and Table 11.

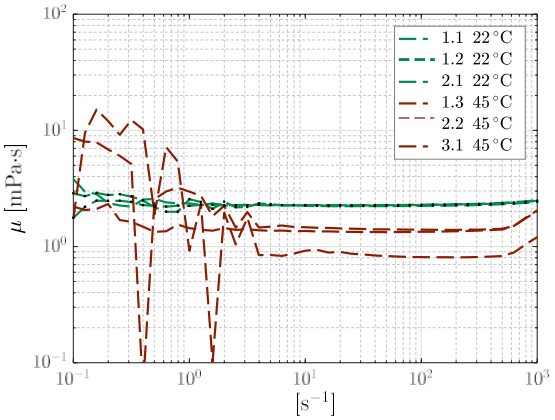

Figure 14: Viscosity of Gascon 469

Table 11: Viscosity of Gascon 469

No.	T [°C]	μ_{10} [mPa s]	μ_{100} [mPa s]
1.1	22	2.267	2.282
1.2	22	2.246	2.240
1.3	45	1.476	1.397
2.2	45	1.359	1.337
3.1	45	0.9185	0.8098

For preliminary rheological investigations, 100 mL FormSeal is prepared by adding 13 mL of a 6 wt% sodium chloride (NaCl) solution to 87 mL GasCon 469 in the procedure stated above. A small sample of this mixture is transferred to a small bottle for gel check and the rest to a larger container for sampling in regular periods. Both beverages are stored in a water bath at 45 °C. Every hour a sample is taken for analysis (Figure 15 and Table 12).

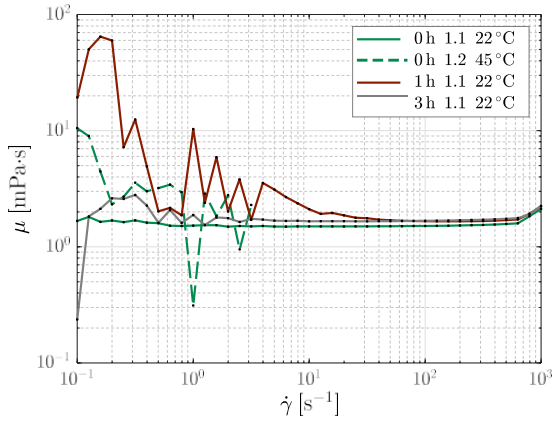

Figure 15: Viscosity alteration of FormSeal during gelation at 45 ◦C – 1st measurement

Table 12: Viscosity of FormSeal during gelation at 45°C – 1st measurement

t_g [h]	[°C]	μ_{10} [mPa s]	μ_{100} [mPa s] 0
	22	1.499	1.511
0	45	*cancelled*	
1	22	2.106	1.662
3	22	1.658	1.673

Apart from a high difficulty to reach a steady state in the rheometer leading measurements to take multiple times longer than usual, no alteration of the viscosity or gelation is recognizable. After leaving the mixture in the water bath overnight, the gel strength of the mixture can be described as an A (Table A1). The experiment is conducted again as given in Figure 16 and Table 13.

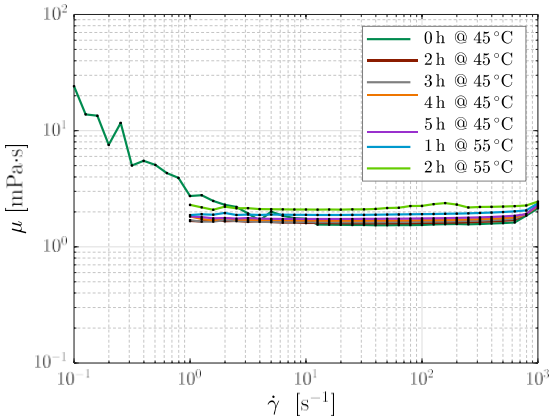

Figure 16: Viscosity alteration of FormSeal during gelation at 45 ◦C–2nd measurement

Table 13: Viscosity of FormSeal during gelation at 45°C – 2nd measurement

t_g [h]	T_g [°C]	μ_{10} [mPa s]	μ_{100} [mPa s]
0	45	1.747	1.543
2	45	1.602	1.599
3	45	1.634	1.642
4	45	1.683	1.690
5	45	1.734	1.753

As previously mentioned, the rheometer can hardly adjust to a steady state in the range of low shear rates. Therefore, all subsequent measurements only analyze the viscosity above a shear rate of 1 s^{-1}. However, the viscosity hardly changes during the five hours of observation or the following two hours at temperatures of 55 °C. The temperature of the water bath is increased every three hours by 10 °C the next day. The experiment is stopped at a temperature of 75 °C with no visible alteration of the mixtures viscosity. Consultation with the manufacturer on the issue revealed that the low end of this product is 50 °C, which should result in a stiff gel within approximately six hours. The companies recommendation includes to check the system's ability for gelation with a fresh sample at 75 °C. At this temperature, gelation should be completed within one hour. However, in a new experiment at 75 °C with a freshly prepared FormSeal sample no gel is present. After checking again two more hours later, a ringing gel has formed. A new test series with a freshly prepared sample at a gelation temperature T_g of 55 °C gives the results plotted in Figure 17.

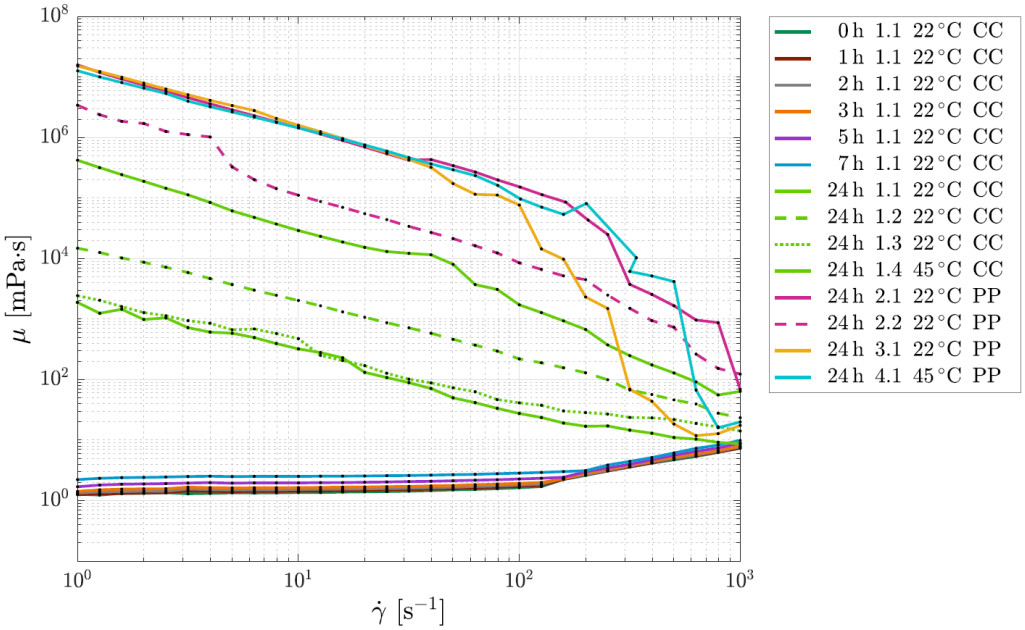

Figure 17: Viscosity alteration of FormSeal during gelation at 55 °C

Table 14: Viscosity of FormSeal during gelation at 55 °C

t_g [h]	No.	μ_{10} [mPa s]	μ_{100} [mPa s]
0	1.1	1.363	1.637
1	1.1	1.435	1.722
2	1.1	1.534	1.820
3	1.1	1.642	1.933
5	1.1	1.964	2.278
7	1.1	2.516	2.849
24	1.1	29 040	1721
24	1.2	2027	219.7
24	1.3	475.1	41.3
24	1.4	321.9	27.58
24	2.1	1 442 000	151 700
24	2.2	111 300	8487
24	3.1	1 591 000	76 530
24	4.1	1 442 000	96 480

During the measurement the gel disintegrates into a grainy mass as subsequent measurements and the visual examination of the sample show. In order to estimate the temperature dependency of FormSeal gelation, 10 mL samples are prepared with 8.7 mL GasCon 469 and 1.3 mL of the 6 wt% NaCl in 25 mL bottles and stored in a water bath at different temperatures while checking for gelation every half hour. The water temperature of the temperature control unit is observed with an additional thermometer. During regular check-ups, the temperature never deviated more than ± 0.5 °C from the set value. Hereby it is very important to stick to the same procedure and use the same bottle sizes for each individual experiment, because the gelation might be related to container size and dimensions.[30] Therefore, the results should not be seen as a fixed gelation time schedule for the application of FormSeal, but more as a guideline for estimating the possible injection time at given temperatures. As the results show, varying the temperature by only 5 °C has a significant impact on the gelation time. For example, the gelation at 75 °C starts after two hours while it is completed at 80 °C within minutes. At 45 °C there is no gelation measurable. At 55 °C the gelation is completed after 23 hours.

Gelation experiments

In a first core flooding experiment, the FormSeal caused severe plugging in the setup, which was filled with brine prior to the gel injection. Therefore, some bulk experiments using different brines were performed. At first, 5 mL of Form Seal was filled in a phial. Then, the same volume of a brine or salt solution was added dropwise to the agent. This experiment was performed for the brine and all its components (NaCl, KCl, CaCl2,MgCl2·6H2O and Na2SO4) at concentrations of 0 g L−1 (deionised water) as a reference and 20 g L^{-1},40 g L^{-1},60 g L^{-1},80 g L^{-1} and 100 g L^{-1}. The results for brine and sodium chloride are pictured in Figure 18. These results are also representative for almost all other tested salt solutions as the gel formed almost always upon contact, except for potassium chloride (KCl) and sodium sulfate (Na2SO4) solutions. For KCl solutions at concentrations of 60 g L^{-1} and higher, the gel forms upon contact with the salt solution. Mixing a KCl solution at a concentration of 20 g L^{-1} with the FormSeal will give a gel after two hours at a temperature of 45 °C. The 40 g L−1 KCl solution forms a gel after 30 minutes at the elevated temperature. The Na2SO4 solutions do not start any gelation at room temperature upon contact with the FormSeal. However, the a gel forms at 45 °C after 30 minutes for the highest salt concentration and ranges to 36 hours for the lowest tested salt concentration of 20 g L^{-1}.

(a) Brine **(b)** Sodium chloride solution

Figure 18: Gelation experiment with FormSeal

5.2.3 PowelGel M2ES

PowelGel M2ES is a microgel produced by Poweltec.

Product description

The provided microgel is an emulsion that is designed for make-up water as synthetic sea water. According to the manufacturer, inversion is obtained easily with KCl brine, typically with a concentration of 2 $_{wt}$%.

- Quantities for 600 g stock solution:

  564.71 g make-up water

  35.29 g microgel emulsion

- Preparation:

  1. Preparation of stock solution:

     1.1. To prepare 600 mL of a concentrated microgel solution, fill the make-up water into a beaker.

     1.2. Install an overhead stirrer and place its paddle in the center of the brine. Run the stirrer at 500 rpm to induce an efficient vortex.

1.3. Add the microgel emulsion.

1.4. Maintain agitation for one hour to obtain a homogeneous solution. At this point the emulsion is reversed and can be diluted easily.

2. Dilution to targeted concentration:

2.1. To prepare 1 L of a diluted microgel solution, fill 925 g make-up water into a beaker or a wide bottom bottle and place the beverage onto a magnetic stirrer. Operate the stirrer at a speed of 300 rpm.

2.2. Add 75 g of the stock solution and maintain the agitation for 15 minutes before usage.

Rheological analysis

At first, a stock solution is prepared once with the recommended potassium chloride solution with a concentration of 2-wt% and once with the brine used for flooding experiments (Section 4.3.2). Its analysis in Figure 19 shows a significant dependency of the brine on its viscosity. Secondly, the stock solution is thinned following the above-mentioned instructions. Given that the delivered microgel concentrate has a concentration of 26.2 % of active material, the thinned solution features 1156 ppm. Its rheological properties are plotted in Figure 20.

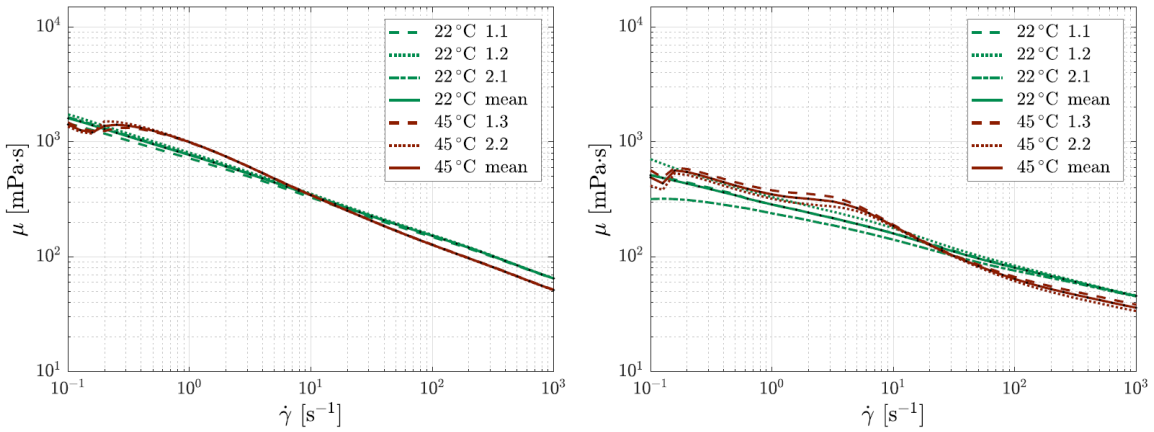

(a) $2\,\mathrm{wt}\%$ KCl (b) $100\,\mathrm{g\,L^{-1}}$ synthetic sea water

Figure 19: Viscosity of M2ES stock solution prepared with different brines

Table 15: Viscosity of M2ES of stock solutions

(a) 2 $_{wt}$% KCl				**(b)** 100 g L^{-1} synthetic sea water			
T [°C]	No.	μ_{10} [mPa s]	μ_{100} [mPa s]	T [°C]	No.	μ_{10} [mPa s]	μ_{100} [mPa s]
22	1.1	328.8	148.8	22	1.1	160.5	81.34
22	1.2	354.7	155.3	22	1.2	177.6	83.95
22	2.1	347.3	153.3	22	2.1	141.1	75.80
22	mean	343.6	152.5	22	mean	159.7	80.36
45	1.3	345.8	127.8	45	1.3	190.0	66.88
45	2.2	343.9	126.7	45	2.2	182.0	61.46
45	mean	344.9	127.3	45	mean	186.0	64.17

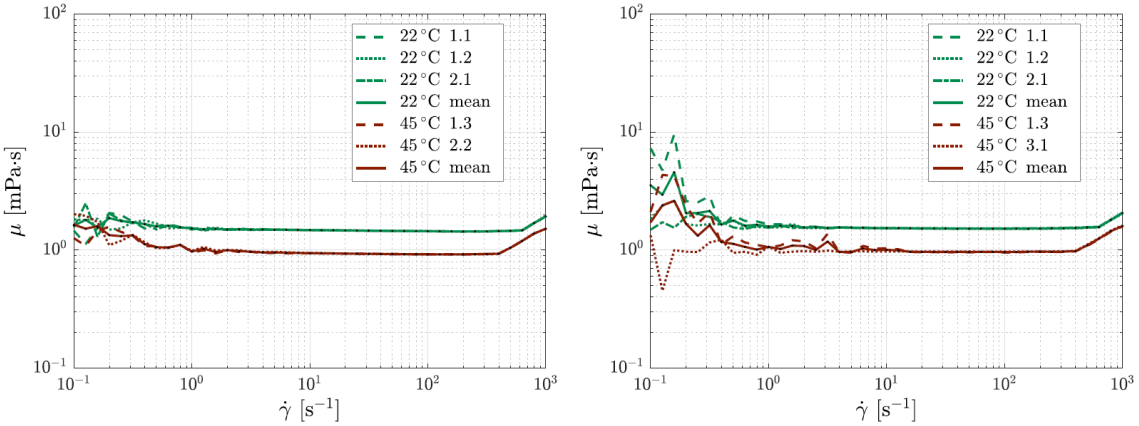

(a) 2 $_{wt}$% KCl (b) 100 g L^{-1} synthetic sea water

Figure 20: Viscosity of M2ES 1156 ppm solution prepared with different brines

Table 16: Viscosity of M2ES 1156 ppm solutions

(a) 2 $_{wt}$% KCl				**(b)** 100 g L^{-1} synthetic sea water			
T [°C]	No.	μ_{10} [mPa s]	μ_{100} [mPa s]	T [°C]	No.	μ_{10} [mPa s]	μ_{100} [mPa s]
22	1.1	1.200	1.131	22	1.1	1.541	1.520
22	1.2	1.030	0.9318	22	1.2	1.524	1.517
22	2.1	1.476	1.446	22	2.1	1.538	1.530
22	mean	1.235	1.170	22	mean	1.534	1.522
45	1.3	0.7647	0.7744	45	1.3	1.037	0.9547
45	2.2	0.9457	0.9215	45	3.1	0.9762	0.9730
45	mean	0.8552	0.8480	45	mean	1.007	0.9277

5.2.4 PowelGel M2EMC

PowelGel M2EMC is a microgel produced by Poweltec.

Product description

The provided microgel is an emulsion that is designed for make-up water as synthetic sea water. According to the manufacturer, inversion is obtained easily with KCl brine, typically with a concentration of 2 $_{wt}$%.

- Quantities for 600 g stock solution:

  564.71 g make-up water

  35.29 g microgel emulsion

- Preparation:

Powelgel M2EMC is a microgel similar to the previously described microgel Powelgel M2ES in Section 5.2.3. It is prepared as described there.

Rheological analysis

At first, a stock solution is prepared once with the recommended potassium chloride solution with a concentration of 2 wt.% and once with the brine used for flooding experiments (Section 4.3.2). Its analysis in Figure 21 shows a significant dependency of the brine on its viscosity. Secondly, the stock solution is thinned following the above mentioned instructions. Given that the delivered microgel concentrate has a concentration of 26.2 % of active material, the thinned solution features 1156 ppm. Its rheological properties are plotted in Figure 22.

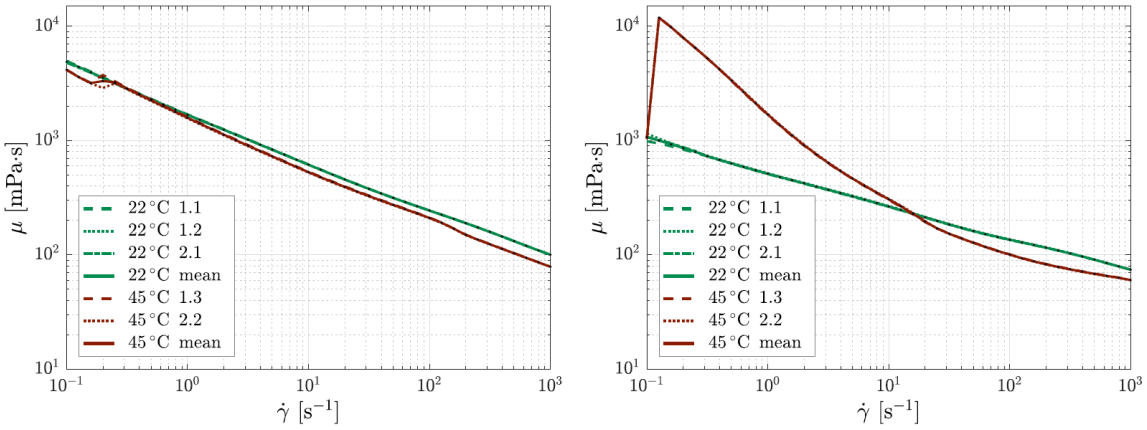

(a) 2 $_{wt}$% KCl **(b)** 100 g L^{-1} synthetic sea water

Figure 21: Viscosity of M2EMC stock solution prepared with different brines

Table 17: Viscosity of M2EMC stock solutions

(a) 2 $_{wt}$% KCl

T [°C]	No.	μ_{10} [mPa s]	μ_{100} [mPa s]
22	1.1	618.7	244.7
22	1.2	613.5	244.7
22	2.1	614.4	243.5
22	mean	615.5	244.3
45	1.3	534.5	212.0
45	2.2	524.5	209.0
45	mean	529.5	210.5

(b) 100 g L^{-1} synthetic sea water

T [°C]	No.	μ_{10} [mPa s]	μ_{100} [mPa s]
22	1.1	263.9	135.3
22	1.2	267.7	129.7
22	2.1	262.9	134.9
22	mean	264.8	133.3
45	1.3	302.1	101.1
45	2.2	309.0	100.0
45	mean	305.6	100.6

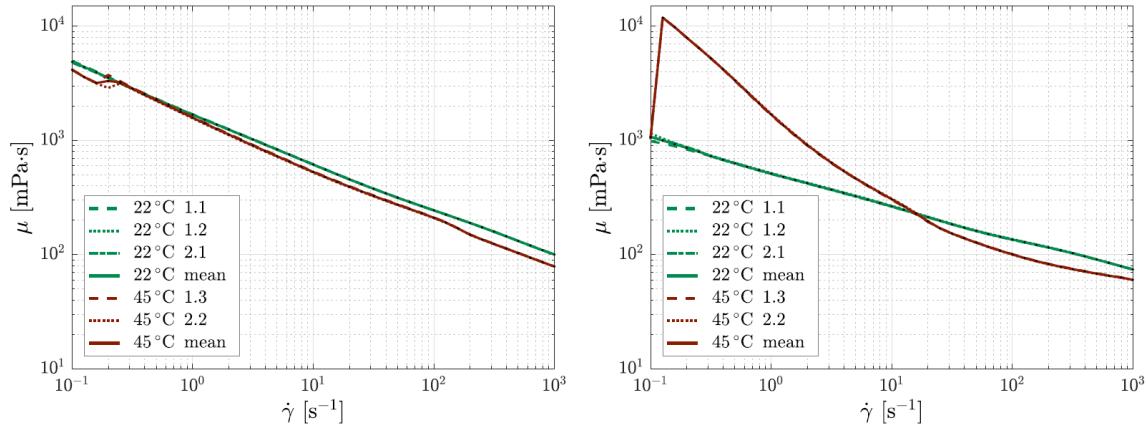

(a) 2 $_{wt}$% KCl **(b)** 100 g L^{-1} synthetic sea water

Figure 22: Viscosity of M2EMC 1434 ppm solution prepared with different brines

Table 18: Viscosity of M2EMC 1434 ppm solutions

T [°C]	No.	μ_{10} [mPa s]	μ_{100} [mPa s]	T [°C]	No.	μ_{10} [mPa s]	μ_{100} [mPa s]
22	1.1	1.378	1.360	22	1.1	1.504	1.502
22	1.2	1.378	1.361	22	1.2	1.504	1.504
22	2.1	1.376	1.361	22	2.1	1.520	1.517
22	mean	1.377	1.361	22	mean	1.509	1.508
45	1.3	0.8689	0.8578	45	1.3	0.9571	0.9532
45	2.2	0.8676	0.8545	45	2.2	0.9633	0.9588
45	mean	0.8634	0.8562	45	mean	0.9552	0.9560

5.2.5 WaterWeb®

WaterWeb® is a relative permeability modifier (RPM) by Halliburton, which ad- sorbs onto the rocks surface were it reduced the effective permeability of water.[31] The WaterWeb® concentration is dependent upon temperature and permeability. For our tests a concentration of 100 gal/Mgal was selected by the manufacturer.

Product description

Below are details about the application handed over by the manufacturer.

- Preparation:
    1. Dilute the HPT-1 agent with 2 % KCl solution to a final concentration of 100 gal/Mgal.
- Application:
    1. Determine the core permeability to brine as deemed appropriate for the particular test.
    2. For the treatment of the core, inject WaterWeb® with a rate of 1 - 5 mL min^{-1}. The injection is stopped either after a total volume injected (TVI) of 10 PV or an increase in differential pressure of 500 psi (34.47 bar), whichever occurs first.
    3. Immediately following treatment, brine flow can be resumed do determine final brine permeability.

5.2.6 LCH5198B

The products LCH5198B and EBO5284B are changing their viscosity under the influence of temperature. As shown in Figure 24 the viscosity increases with temperature until it reaches a peak above the viscosity does not increase any further. The experiment shown in Figure 25b performed with a thinned solution of LCH5198B in brine shows that this change in viscosity is reversible: The viscosity of one sample was measured first at room temperature, then at 45° C and again at room temperature. The viscosity is increased at elevated temperature, but decreases again as soon as the temperature decreases.

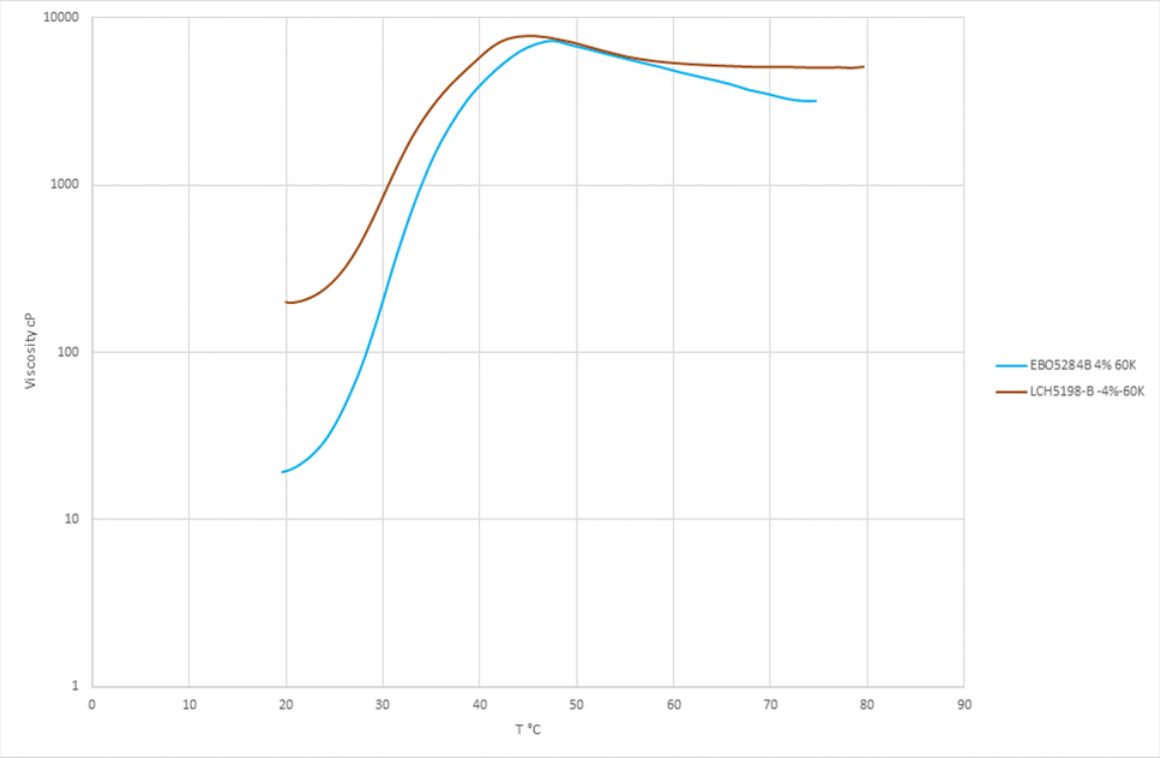

Figure 23: Rheology of LCH5198B and EBO5284B in 60 kppm brine

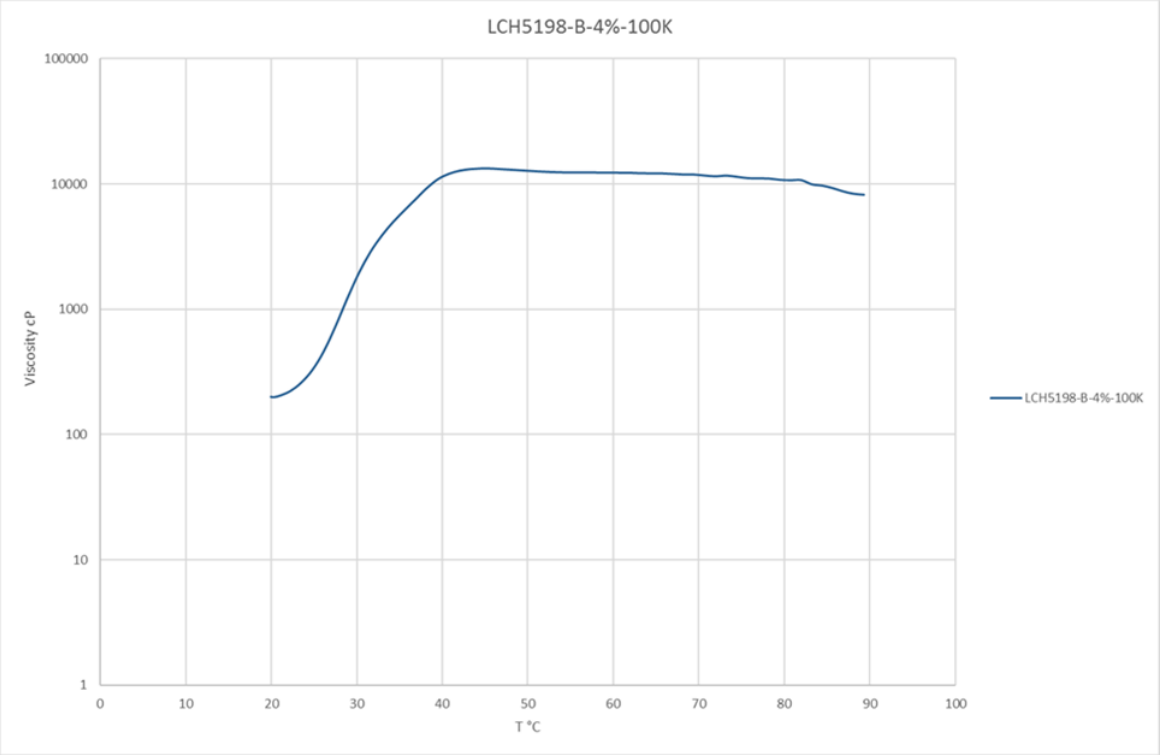

Figure 24: Rheology of LCH5198B in 100kppm brine

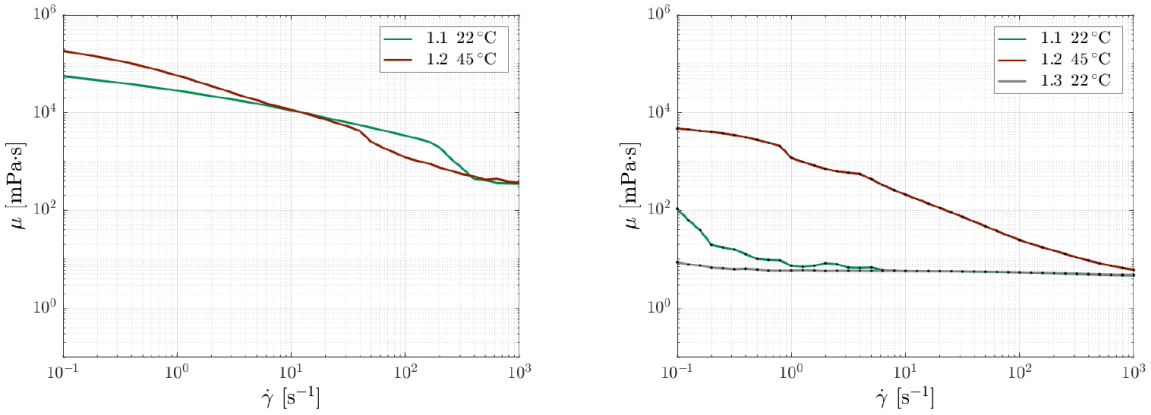

(a) Raw sample **(b)** 4 % solution

Figure 25: Rheology of LCH8198B

5.2.7 EBO5284B

The product EBO5284B is changing its viscosity under the influence of temperature. As shown in Figure 24 the viscosity increases with temperature until it reaches a peak above the viscosity does not increase any further. However, this effect cannot be observed for the thinned solution in brine as shown in Figure 26. It is assumed that the salts in the brine might have a negative influence on the product. The core flooding experiment with this thinned solution did not gave any positive results either.

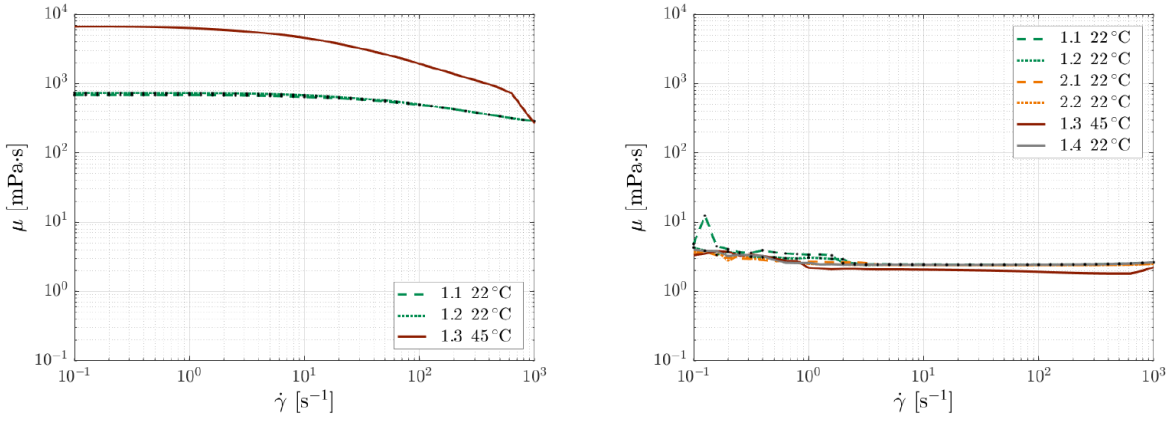

(a) Raw sample **(b)** 4 % solution

Figure 26: Rheology of EBO5284B

6. Work Package – 2 Selection of Products and Literature Update

6.1 Source rock

As source rock for the new micromodel designs serve the Dogger β sandstone on the one hand and the Bentheimer available at the TU Clausthal on the other hand. The image material for the Dogger β sandstone was taken by Wintershall DEA. The µCT scans for the Bentheimer are readily available. Also, the discarded Bentheimer, that was delivered to TU Clausthal, but proved to be unsuitable for core flooding, was scanned by Wintershall DEA. This material was processed as the others to generate new micromodels, but was not chosen for the manufacturing process, as the comparable core material was too fragile and its permeability too low for polemer application.

6.2 Image processing

The design of the rock matrix for the micromodel construction starts with a high resolution µCT from one of the sandstone plugs with a 10 mm diameter and a length of 60 mm. All images delivered are cross-sections along the diameter of the scanned plug. These are stacked to a digital 3D replica of the rock sample to be sliced along the length of the core to receive rectangle 2D images. The workflow is shown in Figure 27 Hundred slices are first converted to binary images and then stacked again for determination of the rock density as seen in the first three sub-images. The density images reveals hidden pores and enables to build a channel network for the 2D micromodel. This network will be laid over the binary grain and pore image to receive the final rock matrix.

The generated rock matrix is used as input image for flow simulation. The software GeoDict simulates water flow though the matrix with along the flow axis in a model with the real properties of the future model and no-slip boundary conditions. In the process, the parameters to generate the rock matrix are adapted until the calculated permeability and porosity of the water flow simulation match the properties of the source rock. After the rock matrix is designed, the lithographic mask needs to be completed. This final lithographic mask has the same dimensions as the manufactured micromodel and features the location of two circles at each end of the rectangular mask that mark the position of the bore holes for fluid inlet and outlet. These boreholes are

connected to the rock matrix with a wide channel opening to a triangular shape. The first millimetres of the rock matrix feature additional channels crossing the matrix in flow direction. These provides an even distribution of injected fluids into the matrix.

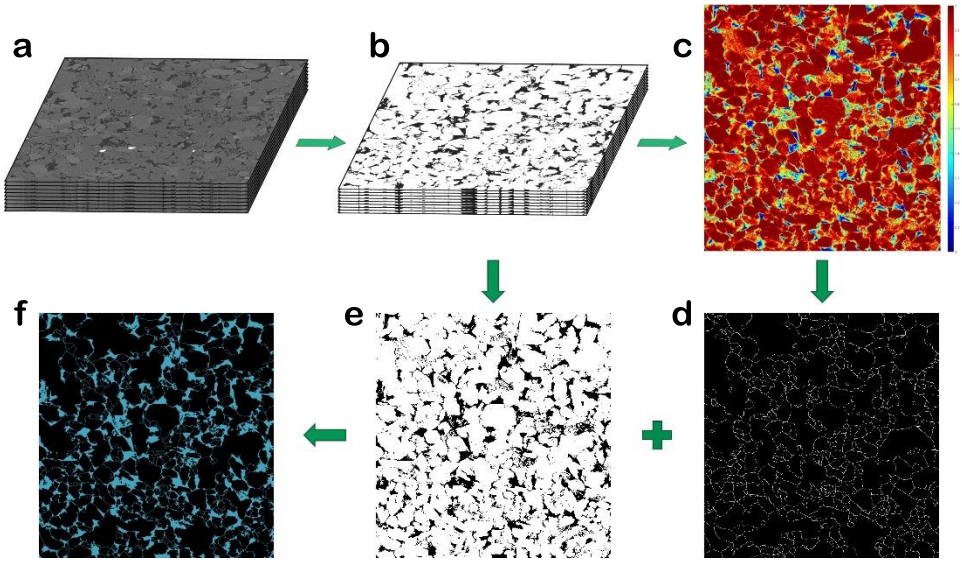

Figure 27: Steps of porous structure design

6.2.1 High and low permeable strata model

To generate a lithographic mask with high and low permeable strata, two different mask are developed. The first one is the one that features the same properties as the rock material in permeability and porosity. It is the same artificial rock matrix used for the homogeneous micromodel design. The second artificial rock matrix is designed by widening the pore openings and enlarge the pores to increase the porosity and permeability. The final micro structure features a permeability ten times higher than the homogeneous design. Both matrices are split in three parts lengthwise and merged back together with two low permeable streaks in the middle and the high permeable streak in the middle.

6.2.2 Fractured micromodel

The fractured micromodel is designed with a novel image processing algorithm developed in MatLab®. It takes the medial axis image displayed in Figure 27d. It is a binary image consisting of a m x n matrix of ones representing a white color or zeros displayed as black color. The user defines two points in this image to be connected and the algorithm corrects at first the position of those points to be relocated into the

next pore channel. Then, the algorithm follows the steps by Eddins to find the path of closest distance in the network[32] as shown in Figure 28. To generate a model with three fractures, three times two opposing start and end points are processed this way.

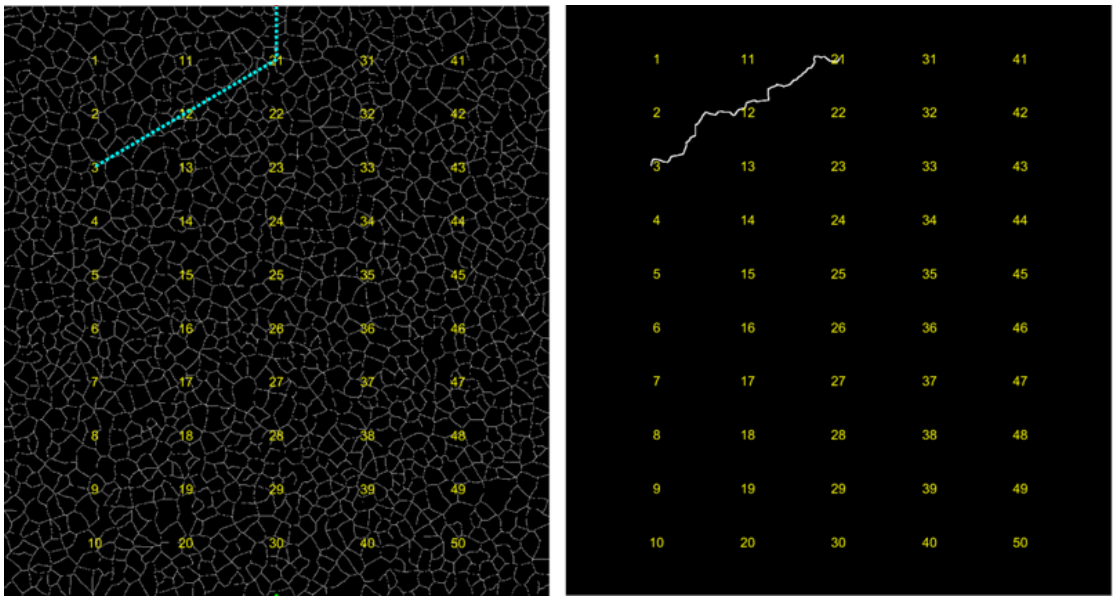

Figure 28: Visualisation of fracture generation in MatLab®.

6.2.3 Final models

Using the method of Gaol and the novel fracture generation algorithm described above, we designed two sets of new micromodel structures derived from µCT im- ages of Bentheimer sandstone and the Dogger β core describes above (Figure 30 and Figure 29). At first, the design of the Bentheimer micromodel with high and low permeable strata was overhauled to achieve a permeability ratio of one to ten. Therefore, the low permeable area has a permeability of 2 Darcy and he high permeable area a permeability of 20 Darcy. A Bentheimer micromodel without any heterogeneities is already available and in use. It features a porosity of 23 % and a permeability of 2 Darcy.[33] Only one novel structure remained to be designed with added fractures of 100 µm width, utilizing the fracture generation algorithm described earlier. It has a slightly increased porosity of 24 % and a permeability of 4.3 Darcy. The set of the three final Bentheimer chips described above are displayed in Figure 31.

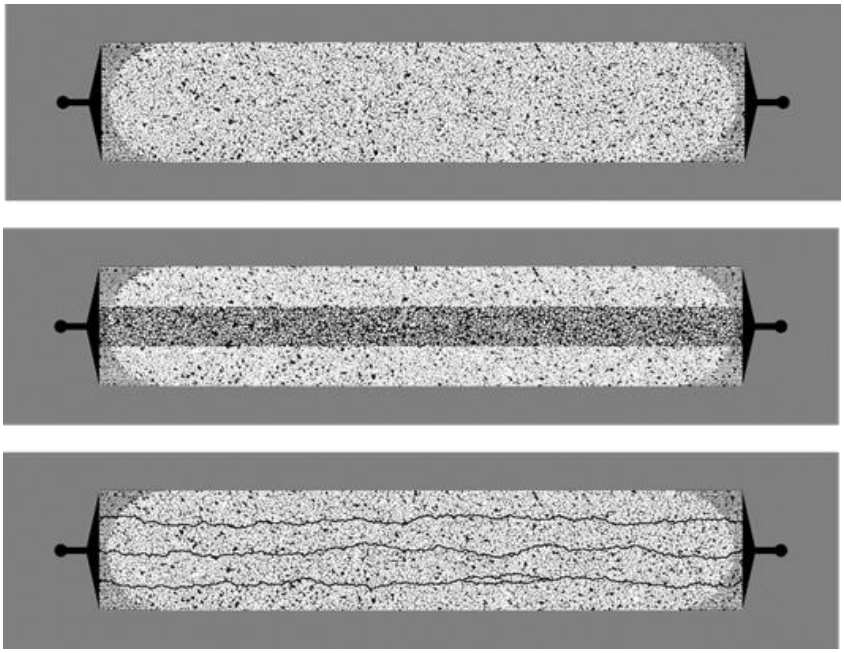

Figure 30: All available designs of micromodels based on µCt images of Bentheimer sandstone – Homogeneous matrix (top),[33] heterogeneous structure with high and low permeable strata with higher difference as published by Gaol et al. (middle) and fractures structure (bottom)

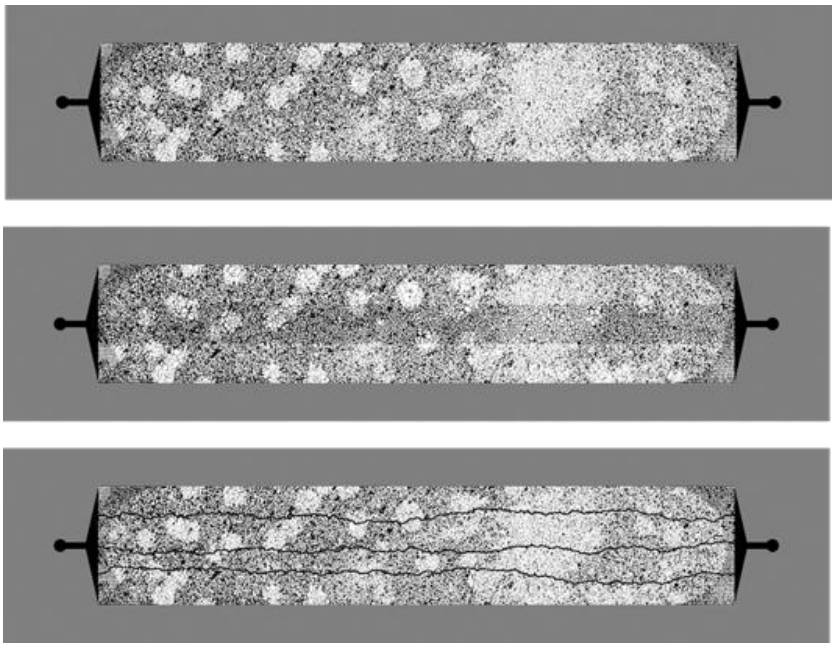

Figure 29: All available designs of micromodels based on µCt images of Dogger β sandstone – Homogeneous matrix (top),[33] heterogeneous structure with high and low permeable strata (middle) and fractures structure (bottom)

The same design process was applied to the µCT image material of the Dogger β sandstone core. Whilst the original rock features a porosity of 30 % and a permeability of 0.2 to 1 Darcy, the computed values for the homogeneous micromodel structure are 29 % and 1.3 Darcy. The high permeable strata added to the first heterogeneous design has a permeability of 13 Darcy, whilst the fractured micro- model features a porosity of 30 % and a permeability of 3.6 Darcy. These fractures have a width of 100 µm. This width can be adjusted as shown in Figure 32. Here the micromodels contain either no fractures or fractures with widths of 45 µm or 90 µm.

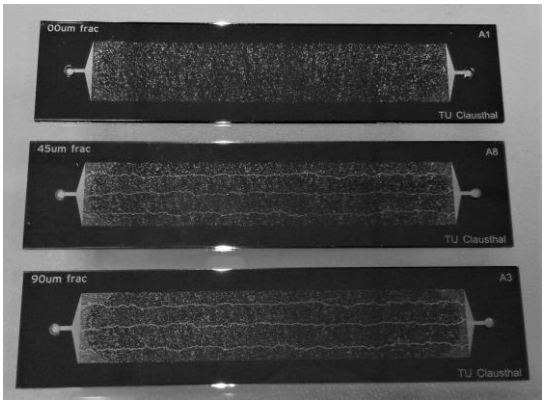

Figure 32: Realistic micromodels with fractures of different widths

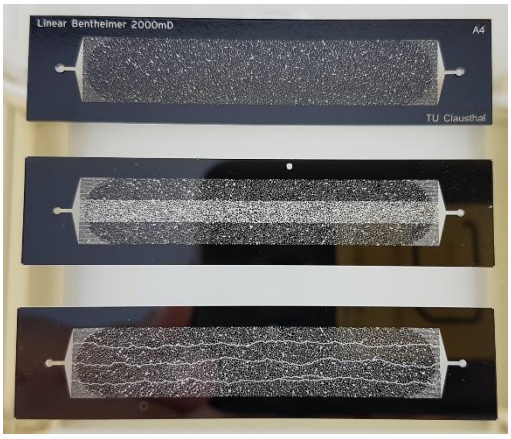

Figure 31: Bentheimer micromodels – Homogeneous matrix (top),[33] heterogeneous structure with high and low permeable strata with higher difference as published by Gaol[33] (middle) and fractured structure (bottom).

In a final set of experiments, the novel Bentheimer micromodels with a high and low permeable strata and with fractures were utilised in single phase experiments to measure the permeability. The computed results in GeoDict® gave a permeability of 4.3 Darcy for the fractured micromodel. The experiment gave almost the same permeability of around 4.2 Darcy (see Figure 33). The experimental results of the permeability measurement with the micromodel with different permeable strata is given in Figure 34.

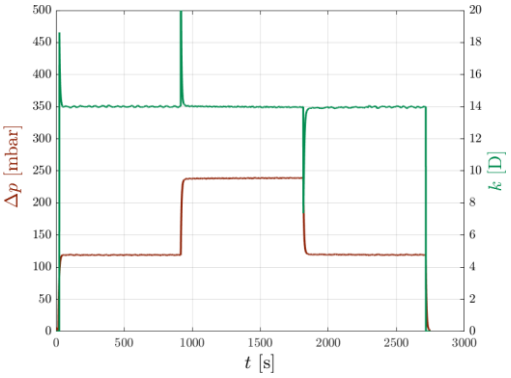

Figure 33: Permeability measurements in fractured Bentheimer micromodel

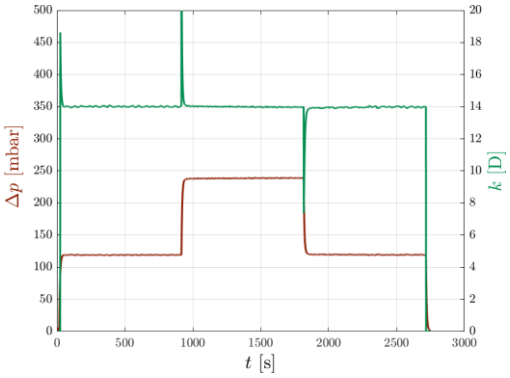

Figure 34: Permeability measurements in fractured Bentheimer micromodel with high and low permeable strata

7. Work Package – 3 Core flooding experiments

In this chapter, we report the results from the core flooding experiments. All experiments are performed with sandstone cores that are 60 mm long and 30 mm in diameter. Before the core is used in a flooding experiment, its porosity ϕ is determined in a helium pycnometer and its permeability to gas kg with nitrogen in a Syroperm gas permeameter. The water permeability kw is measured directly before the core flooding experiment by injecting water into the core at different rates and measuring the differential pressure ∆p. The permeability is calculated according to Darcy's law:

$$Q = \frac{k \,.\, A}{\mu} \left(\frac{\Delta p}{\Delta x}\right) \ldots (3)$$

Here:

Q : flow rate [$m^3.s^{-1}$]
k : permeability [m^2]
A : area [m^2]
μ : fluid viscosity [Pa.s]
Δp : differential pressure [Pa]
Δx : length [m]

For core flooding experiments, the core has to be sealed tight into a sleeve to shut of any fluid flow bypassing the rock material or to prevent leakage. Therefore, the core is placed into a flexible Viton™ sleeve (Figure 35a). Viton™ consists of a fluoropolymer elastomer with high resistance to temperature and chemicals. Both ends are sealed with gaskets that allow fluid flow through two capillaries at each end as seen in Figure 35b. One capillary will be connected to a pressure sensor and the other will be connected either to the fluid injecting pump on one end and to the effluent at the other end. This set up enables the fluid flow through the core and measurement of the differential pressure. To disable any fluids from bypassing the rock between its rough surface and the walls of the tube, this part of the setup has to be pressurized for complete sealing. Therefore, the sleeve with the sealed-in core is placed into a closed steal pipe, which is filled with water and set under a pressure of 150 bar. This Hassler Cell is horizontally mounted into a heating cabinet and connected via the capillaries with the pressure sensors and the fluid transporting pipes (Figure 35c).

(a) Core placed in Viton™ sleeve

(b) Sleeve sealed with gaskets connected to capillaries (*bottom*) and pressure cell (*top*)

(c) Mounting of pressure cell in a heating cabinet

Figure 35: Core flooding setup

7.1 WaterWeb

For the core flooding experiment, the WaterWeb is prepared as described in part 5.2.5 and the Dogger β 1228 core mounted into the Hassler cell. Then, the core is flushed several times with toluene and methanol for cleaning and removing any gas phase. It is flushed with water and brine before the permeability is measured with brine first at room temperature and then at 45 °C. For the treatment of the core, 10 PV of the diluted WaterWeb solution are injected at a rate of 1 mL min−1. After the treatment, the permeability is measured again. The results are displayed in Table 19.

Table 19: Results from Water Web core flooding experiments

Q [mL min−1]	Δpi [mbar]	Δpe [mbar]	ki [mD]	ke [mD]
0.25	1.9	3.2	2108	1251
0.50	3.8	13.3	2108	602
0.75	5.5	14.8	2184	811
1.00	7.4	16.3	2179	982

7.2 Form Seal

A Bentheimer core is flushed several times with toluene and methanol for cleaning and removing any gas phase. It is then saturated with deionized water for the experiment instead of brine. Any experiment performed with a brine saturated core failed due to plugging. Bulk experiments with the Form Seal agent and brine showed full gelation to a rigid gel upon contact as described in section 5.2.2. This spontaneous gelation lead to severe plugging of the setup. Therefore, any experiment has to be performed in a set up and core flushed with fresh water.

Table 20: Results from Form Seal core flooding experiments

Q [mL min−1]	Δpi [mbar]	Δpe [mbar]	ki [mD]	ke [mD]
0.25	11	1137	364	3.5
0.50	16	1220	501	6.6
0.50	-	1229	-	6.5
1.00	30	-	545	-

7.3 M2ES

The core flooding experiment of PowelGel M2ES was performed using a Bentheimer core plug at 45 °C. At first, the core is encased into the Hassler cell. A radial pressure of 30 bar is supplied to the core. The whole set up including the core and the pressure sensor system is flushed with deionized water. Then, CO_2 is injected for at least 30 minutes, which is replaced with deionized water. The permeability is first measured at room temperature and then again at reservoir temperature. The PowelGel is prepared as described in section 5.2.3. Up to two pore volumes of the gel is injected into the core. To restore the injectivity, the pumps and the system excluding the core is flushed with water and then 1 mL injected into the core. The core is shut in according to the instructions given for each product. Finally, the permeability is measured again to determine the permeability reduction. The experiment is performed two times. The results are given in Figure 36 and Figure 37.

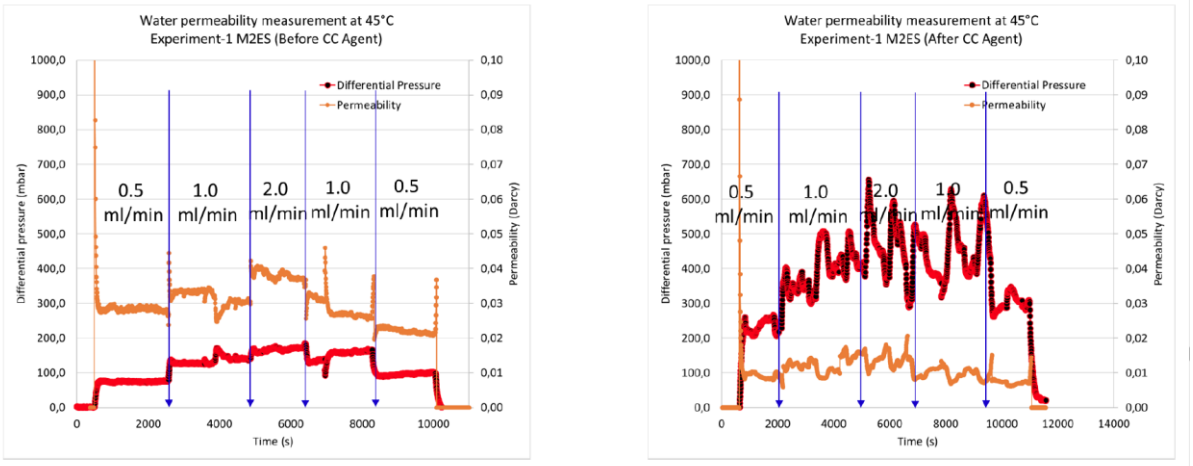

(a) Before M2ES application **(b)** After M2ES application

Figure 36: Permeability measurements before and after application of M2ES – Experiment I

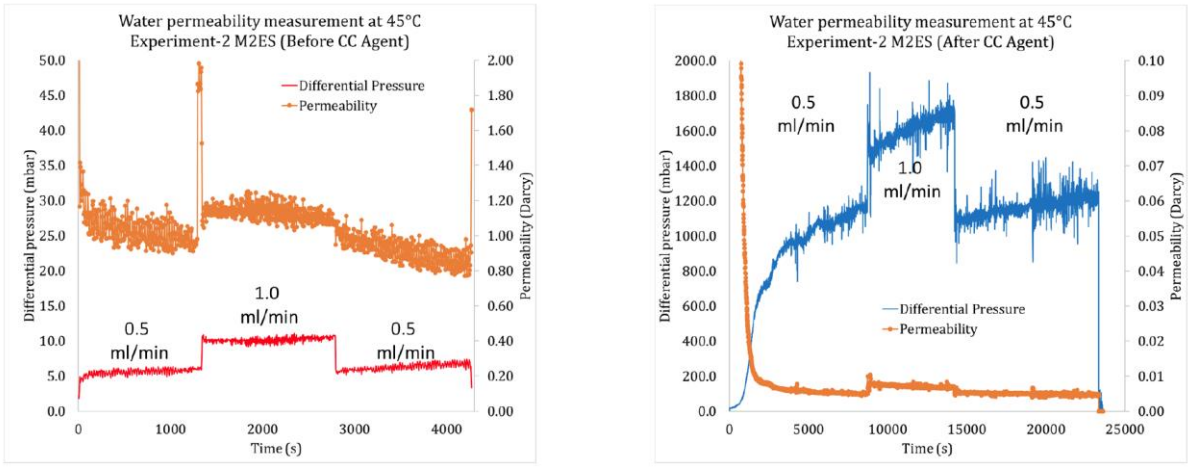

(a) Before M2ES application **(b)** After M2ES application

Figure 37: Permeability measurements before and after application of M2ES – Experiment II

7.4 M2EMC

The procedure for PowelGel M2EMC is the same as for the previous gel in sec- tion 7.3. The results are given in Figure 38 and Figure 39.

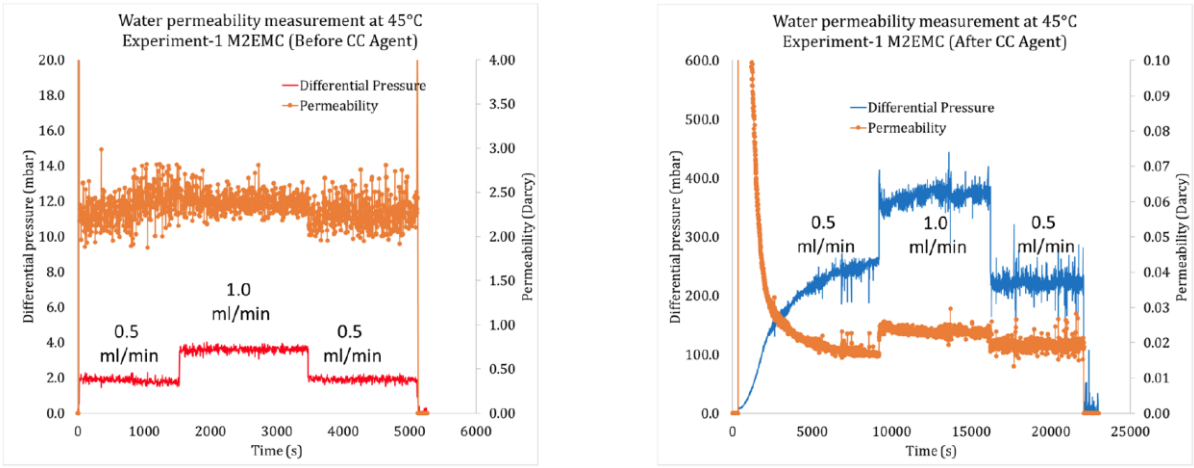

(a) Before M2EMC application (b) After M2EMC application

Figure 38: Permeability measurements before and after application of M2EEMC – Experiment I

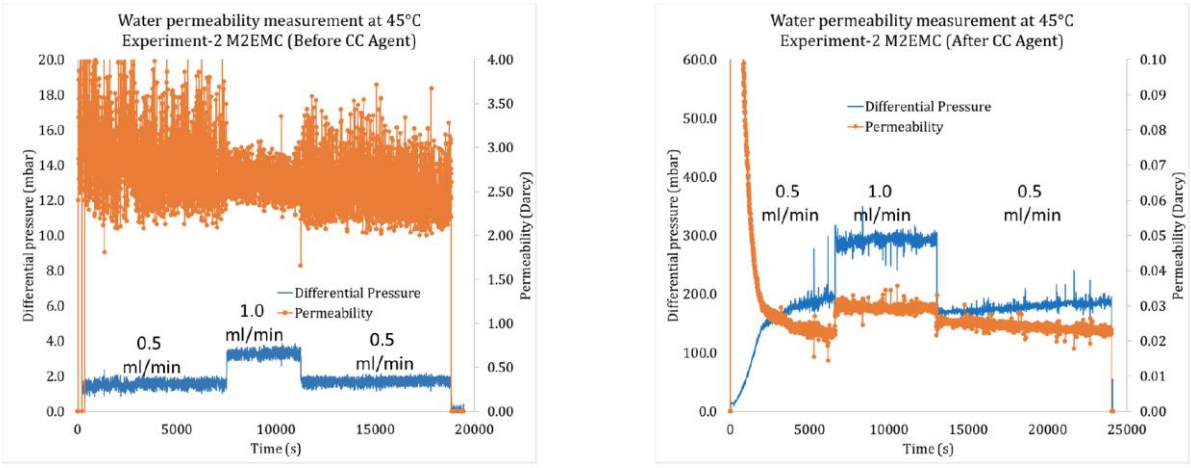

(a) Before M2EMC application (b) After M2EMC application

Figure 39: Permeability measurements before and after application of M2EMC – Experiment II

7.5 H2Zero™

The core flooding experiment of H2Zero™ was performed using a Bentheimer core plug at 45 °C. At first, the core is encased into the Hassler cell. A radial pressure of 30 bar is supplied to the core. The whole set up including the core and the pressure sensor system is flushed with deionized water. Then, CO_2 is injected for at least 30 minutes, which is again replaced with deionized water. The permeability is first measured at room temperature and then again at reservoir temperature. It is around 2.1 D. The H2Zero™ is prepared by dissolving 3 g KCl and 50 mL HZ-30 in 146 g distilled water. The mixture is stirred for at least 30 minutes before adding 4 mL HZ-20. 10 PV of the so prepared H2Zero™ is injected into the core at a rate of 1 mL min−1. To restore the injectivity, the pumps and the system excluding the core is flushed with water and then 1 mL injected into the core. The core is shut in for 24 hours. Finally, the permeability was about to be measured again, but no flow could be re-established. The inlet pressure was increased stepwise up to 150 bar without any measurable flow.

7.6 EBO5284B

For this experiment, the Bentheimer core was prepared as before by injection of deionized water, flushing with CO_2 and again injection of water. The permeability is first measured at room temperature and then again at reservoir temperature. The EBO5284B is thinned to 4 % using brine. This thinned solution is injected for 10 PV at a rate of 1 mL min−1. To restore the injectivity, the pumps and the system excluding the core is flushed with water and then 1 mL injected into the core. The core is shut in for 24 hours. Finally, the permeability was measured again without any change in the pressure data prior to the treatment.

7.7 LCH5198-B

For this experiment, the Bentheimer core was prepared as before by injection of deionized water, flushing with CO2 and again injection of water. The permeability is first measured at room temperature and then again at reservoir temperature to be above 2 Darcy. A precise measurement of the permeability is not possible as the pressure data is covered by the noise of the measurement. The LCH5198-B is thinned to 4 % using brine. This thinned solution is injected for 10 PV at a rate of 1 mL min−1. To restore the injectivity, the pumps and the system excluding the core is flushed with water and then 1 mL injected into the core. The core is shut in for 24 hours. Finally, the permeability was measured again. The results are plotted in Figure 40. At first, the differential pressure is increased rapidly until some of the gel is flushed out of the core. Then, the pressure decreases and the permeability reaches a stable level at 200 mD.

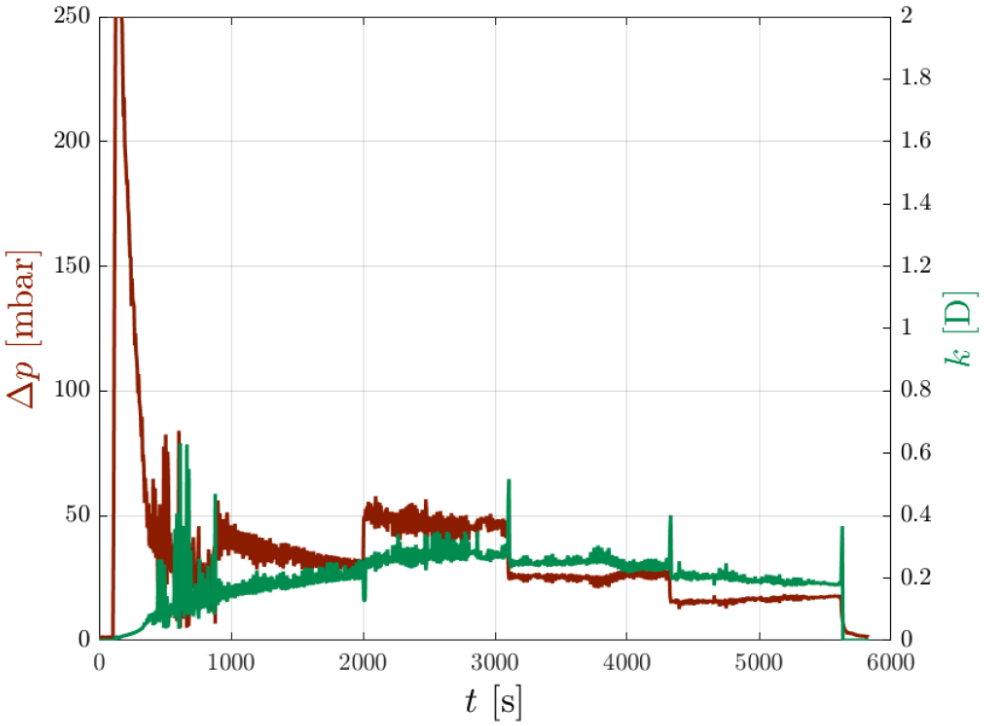

Figure 40: Permeability measurement after treatment with LCH5198-B

7.8 Summary of core flooding experiments

The results of all performed core flooding experiments are displayed in Table 21.

Table 21: Results from all core flooding experiments

Polymer/Gel	Manufacturer	k_i [mD]	k_e [mD]	Permeability reduction [%]
WaterWeb	Halliburton	2110	600	72
FormSeal	Halliburton	545	7	98.7
H2Zero	Halliburton	2000	0	100
M2ES	PowelTec	950	4	99.6
M2MEC	PowelTec	2600	21	99.2
EBO5284B	SNF	>2000	>2000	0
LCH5198-B	SNF	>2000	200	>90

8. Work Package – 4 Microfluidic experiments

In this chapter we present the results of the microfluidic experiments. All presented single phase flooding experiments follow the same procedure:

1. Flushing the micromodel and the whole set up including the pressure sensor system to with distilled water.
2. Measurement of water permeability at 45°C
3. Preparation of the conformance control agent as described in the instructions given with each product.
4. Injection of 10 PV of the agent into the micromodel
5. Shut in the micromodel for 24 hours.
6. Measurement of water permeability at 45°C.

8.1 WaterWeb single-phase flow

Figure 41 shows the result from the microfluidic experiment with WaterWeb. The permeability is slightly reduced by 9 % from 1.65 to 1.5 Darcy. Under the microscope, the particles of the agent are visible (Figure 42).

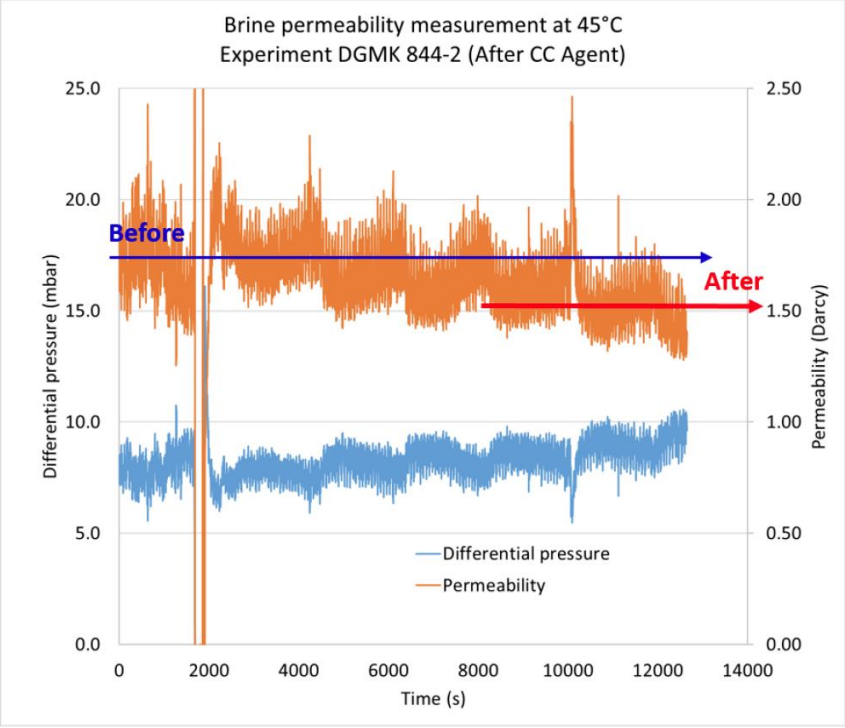

Figure 41: Results from microfluidic experiment with WaterWeb

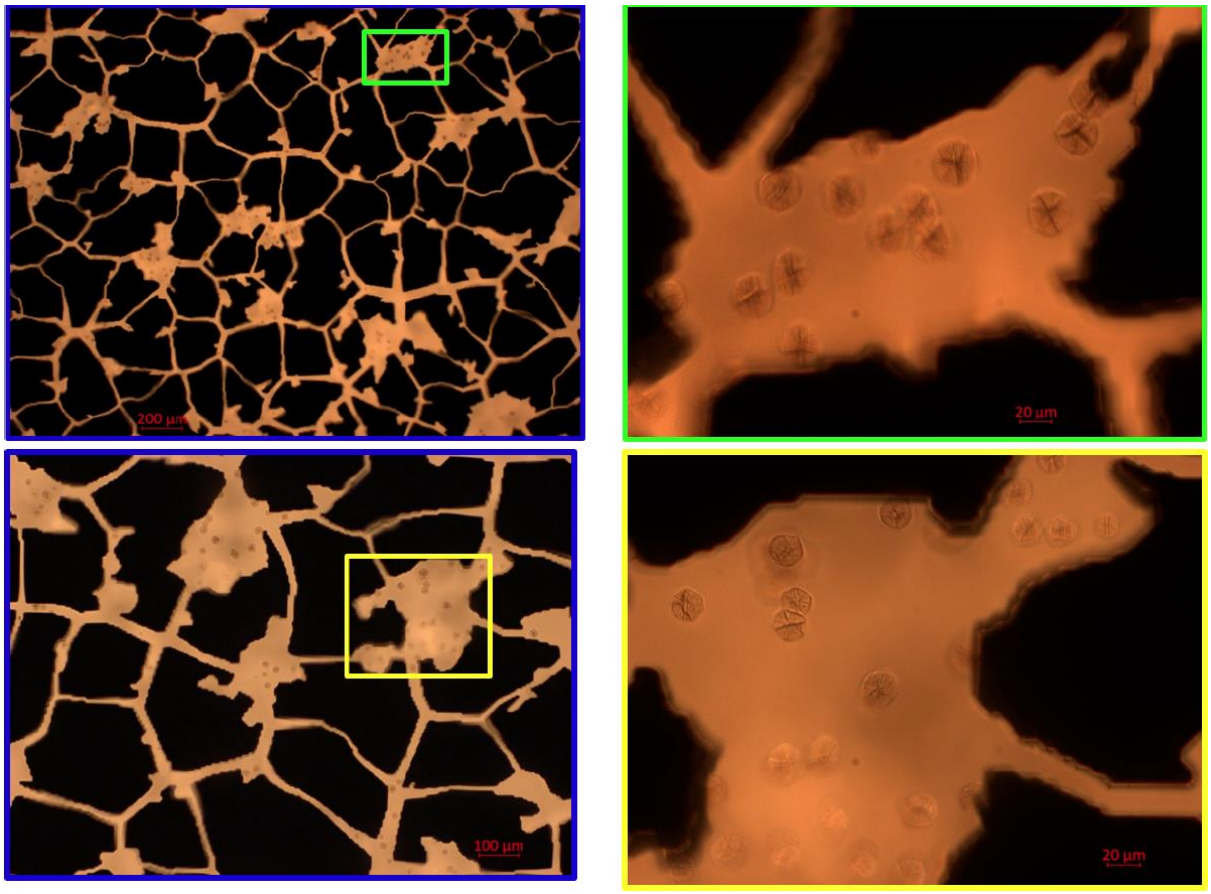

Figure 42: Image of focus micromodel area obtained with objective 5x Brightfield transmitted light (left) and objective 40x Brightfield transmitted light (right)

8.2 M2ES single-phase flow

The results from the microfluidic experiment with M2ES in the fractured micromodel are displayed in Figure 43. The permeability is reduced by 17 % from 14.8 Darcy to 12.2 Darcy. Figure 44 shows the results from the same experiment performed in a micromodel with high and low permeable streaks. The permeability is reduced by 25 % from 11.6 Darcy to 8.74 Darcy.

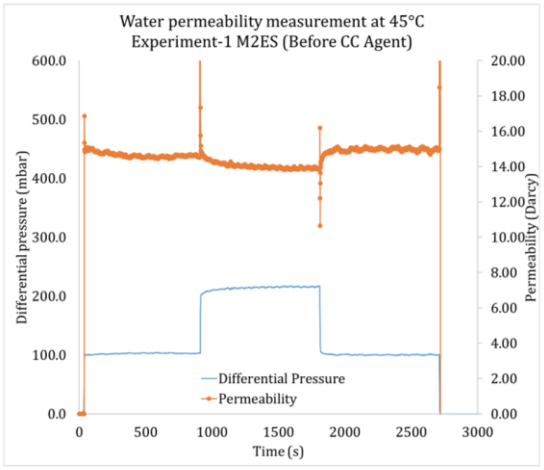

(a) Before M2ES application

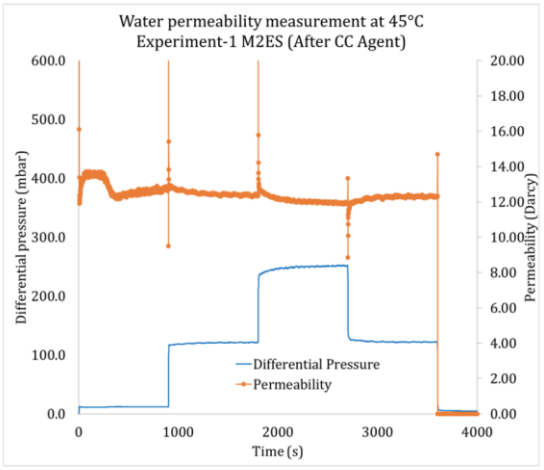

(b) After M2ES application

Figure 43: Permeability measurements before and after application of M2ES – Experiment in fractured micromodel

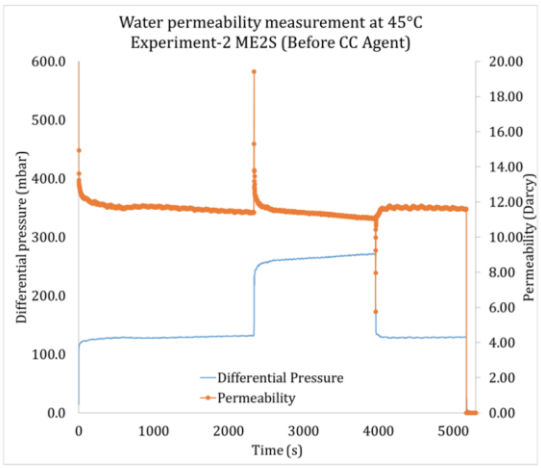

(a) Before M2ES application

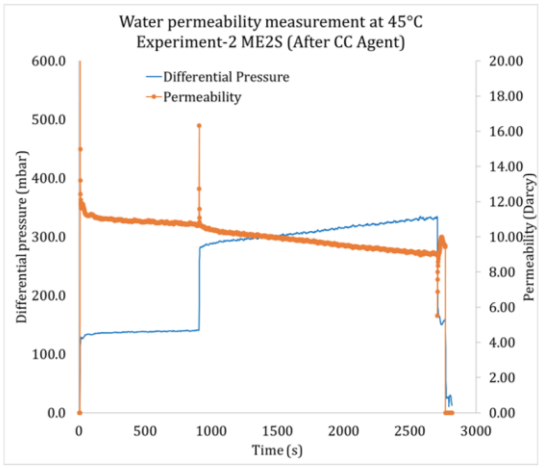

(b) After M2ES application

Figure 44: Permeability measurements before and after application of M2ES – Experiment in high and low permeable micromodel

8.3 M2EMC single-phase flow

The results from the microfluidic experiment with M2MEC in the fractured micromodel are displayed in Figure 45. The permeability is reduced by 27.4 % from 13.3 Darcy to 9.65 Darcy. Figure 46 shows the results from the same experiment performed in a micromodel with high and low permeable streaks. The permeability is reduced by 23 % from 14.8 Darcy to 11.4 Darcy.

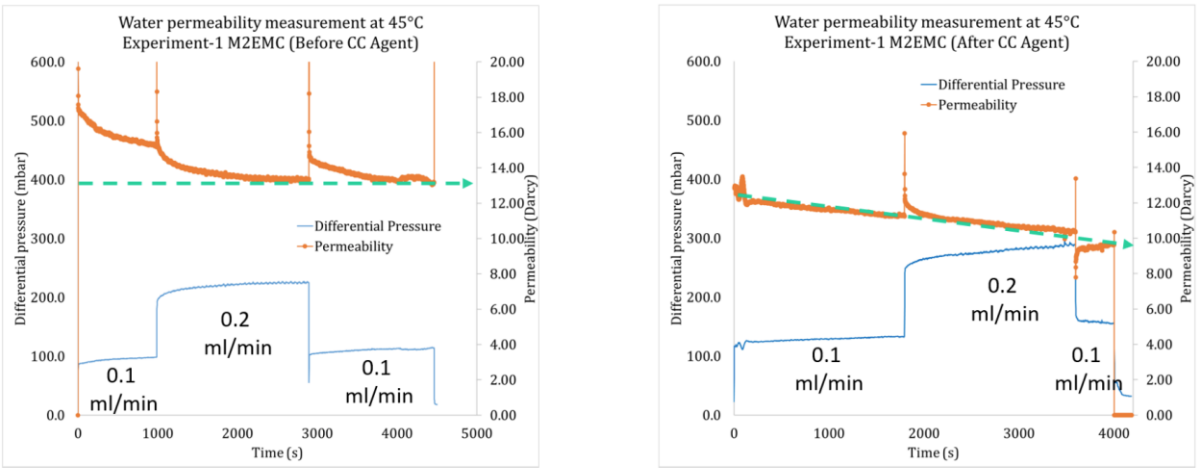

(a) Before M2EMC application (b) After M2EMC application

Figure 45: Permeability measurements before and after application of M2EMC – Experiment in fractured micromodel

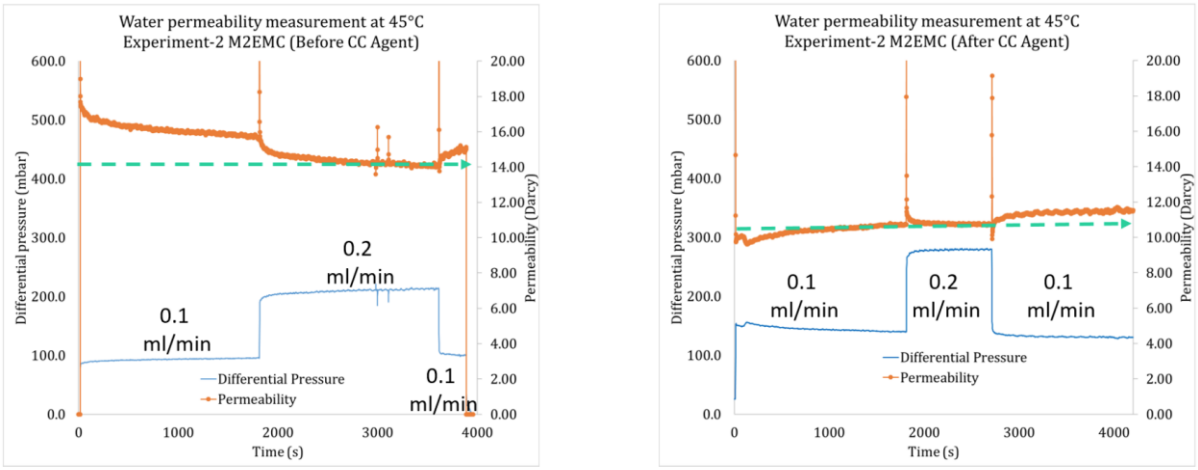

(a) Before M2EMC application (b) After M2EMC application

Figure 46: Permeability measurements before and after application of M2EMC– Experiment in high and low permeable micromodel

8.4 LCH5198 single-phase flow

The results from the microfluidic experiment with M2MEC in the fractured mi- cromodel are displayed in Figure 47. The permeability is reduced by 14 % from 14.8 Darcy to 12.7 Darcy. Figure 48 shows the results from the same experiment performed in a micromodel with high and low permeable streaks. The permeability is reduced by 19.7 % from 7.7 Darcy to 6.2 Darcy.

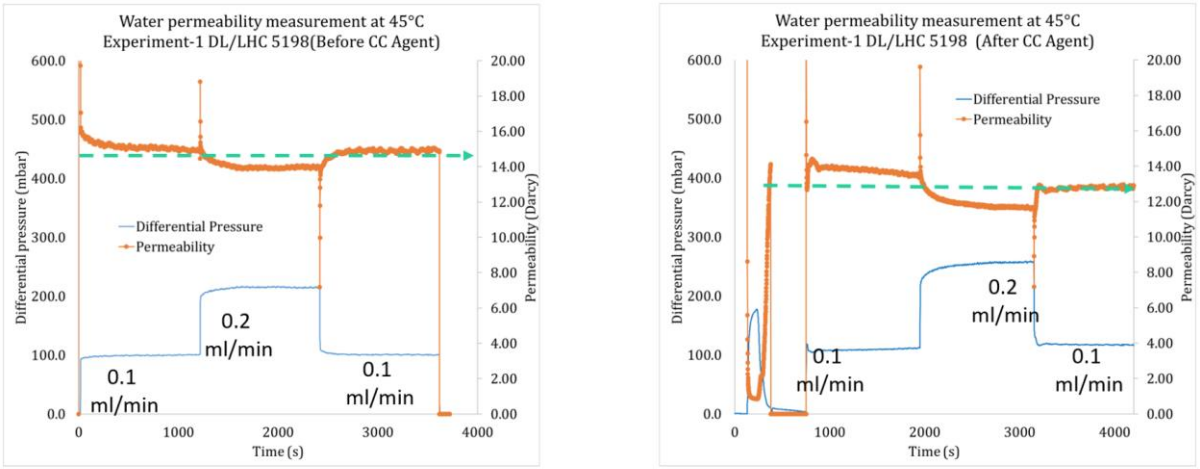

(a) Before LCH5198 application (b) After LCH5198 application

Figure 47: Permeability measurements before and after application of LCH5198– Experiment in fractured micromodel

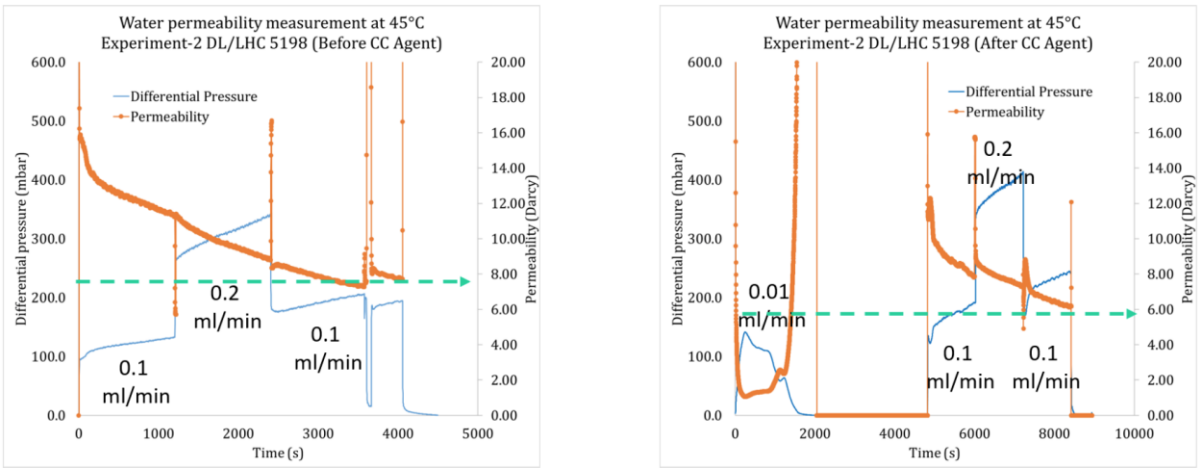

(a) Before LCH5198 application (b) After LCH5198 application

Figure 48: Permeability measurements before and after application of LCH5198– Experiment in high and low permeable micromodel

8.5 WaterWeb two-phase flow

In this chapter, we present the results of a two-phase microfluidic experiment with WaterWeb. The presented flooding experiment follows the following procedure:

1. Preparation
2. Oil initialisation
3. Injection of brine (water flooding) followed by bumb rates
4. Brine permeability measurement
5. Injection of WaterWeb for 10 to 20 PV and shut in for 24 hours
6. Brine permeability measurement

Figure 49 shows the progress of the water flood with bumb rates. At first, brine enters the micromodel (a) and flows through it until it reaches the outlet (b). Sub-figure c shows the micromodel at the end of brine injection with a rate equivalent to 1 feet per day, Sub-figure d at the end of the injection with a rate equivalent to 10 feet per day and Sub-figure e at the end of the injection with a rate equivalent to 200 feet per day.

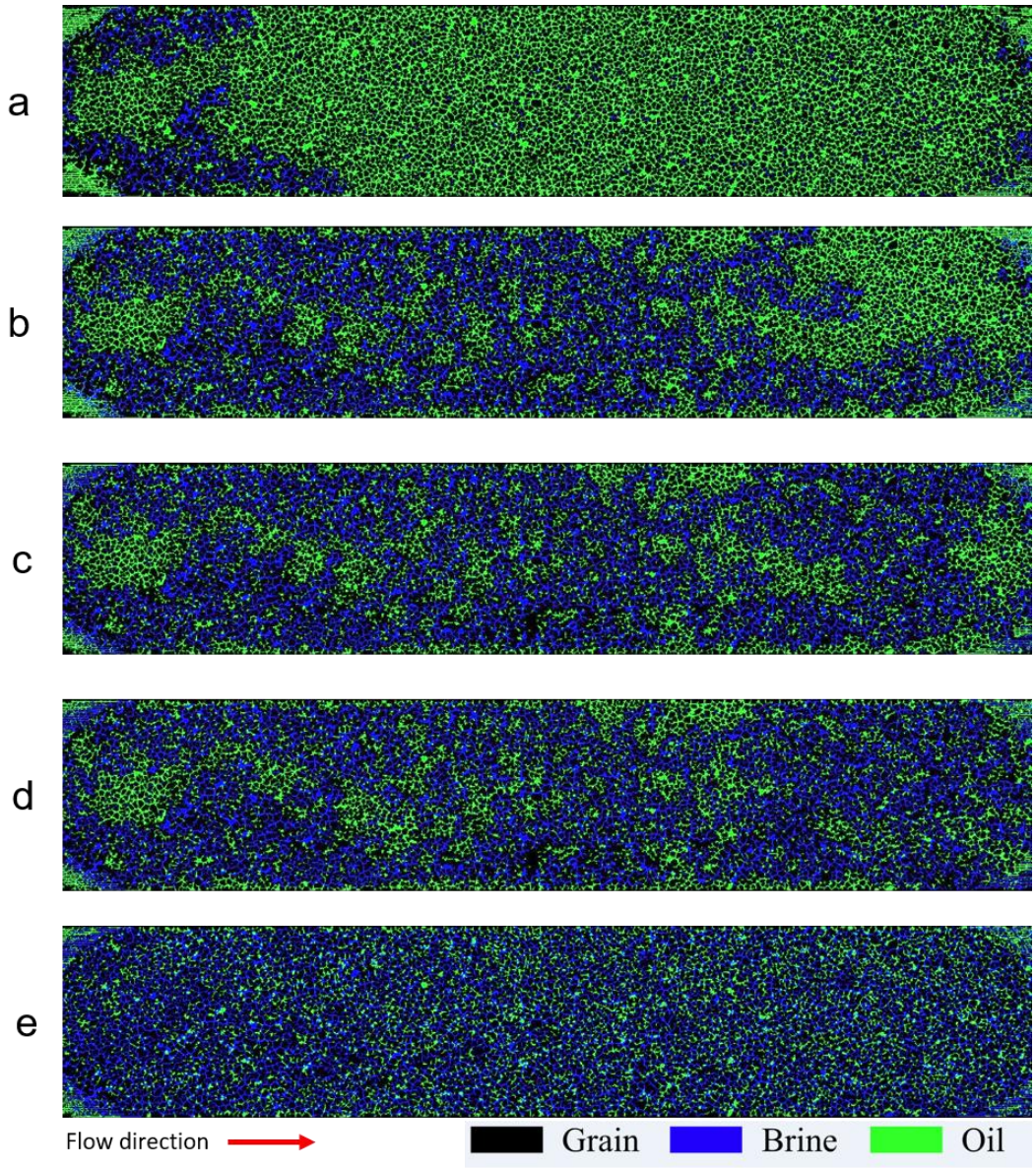

Figure 49: Images of two-phase flow microfluidic experiment with WaterWeb

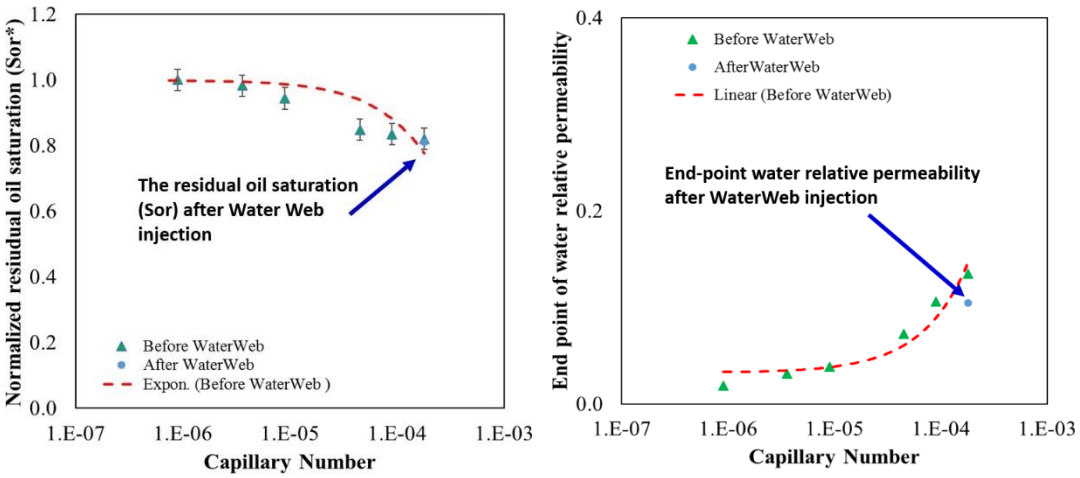

Figure 50: The capillary desaturation curve (left) and end-point water relative permeability relationship to capillary number.

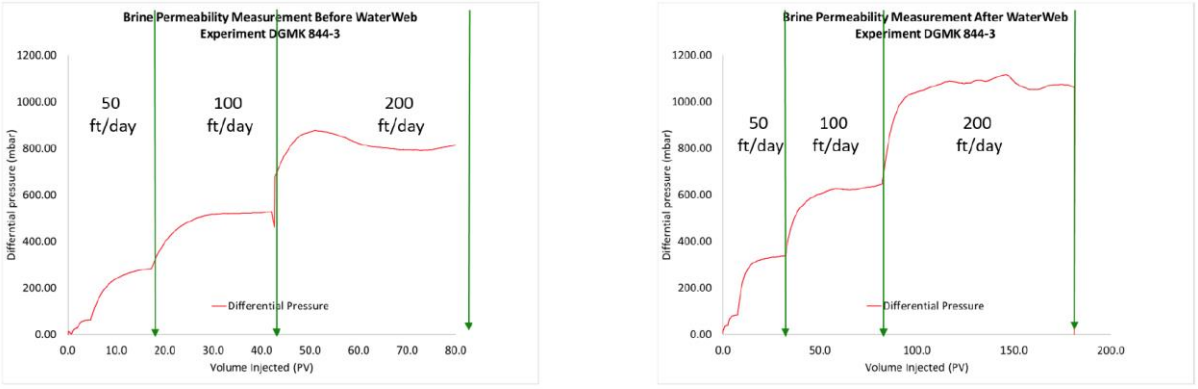

(a) Before WaterWeb application (b) After WaterWeb application

Figure 51: Permeability measurements before and after application of WaterWeb in two phase flooding experiment

8.6 Summary of microfluidic experiments

The results of all performed flooding experiments are displayed in Table 22.

Table 22: Results from all microfluidic flooding experiments

Polymer/Gel	Micromodel type	k_i [D]	k_e [D]	Permeability reduction [%]
WaterWeb	Homogeneous Bentheimer	1.65	1.5	9
M2ES	Fracture	14.8	12.3	17
M2ES	High/low perm	11.6	8.74	25
M2EMC	Fracture	13.3	9.65	27.4
M2EMC	High/low perm	14.8	11.4	23
LCH5198	Fracture	14.8	12.7	14
LCH5198	High/low perm	7.7	6.2	19.7

9. Conclusion

In recent years the most noticeable developments in conformance control research were the improvement of stability and the reduction of the environmental impact. Polymers and gels with a higher resistance towards salinity, temperature and pH aim to be applied in more complex reservoirs. This is achieved for example through the utilization of biopolymers or the combination of polymer systems with nano-particles. There is also an increased interest in Microbial Enhanced Oil Recovery (MEOR) as a cost efficient alternative.

New micromodels that feature common heterogeneities like fractures and high and low permeable streaks were designed, manufactured and tested in single-phase microfluidic experiments with relative permeability modifiers and other conformance control agents. These products were also tested in single-phase core flooding experiments alongside in situ gelling polymer and colloidal gels. Almost all products showed an effective reduction in water permeability here. In some cases, the water flow was shut off completely. The single-phase experiments of all products, both in core and micromodels are excellent and promising, particularly the core plug permeability reduction. This result encourages us to understand the gel's mechanisms, especially in two-phase conditions.

In comparison with analogous core flooding experiments in Bentheimer or Dogger beta sandstone samples, the micromodels showed a significant lower reduction of permeability than the core samples. This might be caused by the different surface to volume ratio of micromodels with their 2D structure compared to the three dimensional core samples and the lower adsorption in micromodels compared to real rocks. Furthermore, the smooth surface in the micromodels compared to the rough surfaces of the sandstone might have an effect on the results. Another difference is the overall morphology: while the micromodels featured either fractures or high and low permeable streaks, the used sandstone sample featured a homogeneous structure.

References

1. J. Wegner, Investigation of Polymer Enhanced Oil Recovery (EOR) in Micro- fluidic Devices that resemble Porous Media –- An Experimental and Numerical Approach, Shaker Verlag, Aachen, 2015. ISBN:978-3-8440-3520-9
2. P. L. Gant, W. G. Anderson, SPE Form Eval 1988, 3, 131 – 138.
3. D. G. Hatzignatiou, R. Askarinezhad, N. H. Giske, A. Stavland, SPE Pro- duction& Operation 2016, , 337–350.
4. D. Zhu, J. Hou, Q. Wei, Y. Chen, K. Peng, Development of a High- Temperature Resistant Polymer Gel System for Conformance Control in Jidong Oilfield presented at the SPE/IATMI Asia Pacific Oil & Gas Con- ference and Exhibition, 17th–19th October 2017, Jakarta, Indonesia, Society of Petroleum Engineers, 2017. DOI:SPE-186235-MS
5. D. A. Elhossary, W. Alameri, E. W. Al-Shalabi, Experimental Investigation of Biopolymer Rheology and Injectivity in Carbonates presented at the Offshore Technology Conference, 4th May, , 2020. DOI:OTC-30680-MS
6. B. Leonhardt, B. Ernst, S. Reimann, A. Steigerwald, F. Lehr, Field Testing the Polysaccharide Schizophyllan: Result of the First Year presented at the SPE Improved Oil Recovery Symposium, Tulsa, Oklahoma, USA, 12th–16th April 2014, Society of Petroleum Engineers, 2014. DOI:SPE-169032-MS
7. E. Alagic, N. Dopffel, G. Bødtker, B. Hovland, S. Mukherjee, P. Kumar, M. Dillen, Biodegradation Mitigation and Protection Strategies for the Biopoly- mer Schizophyllan presented at the SPE Europec featured at 82nd EAGE Conference and Exhibition, Society of Petroleum Engineers, 2020. DOI:SPE- 200562-MS
8. O. Ogezi, J. Strobel, D. Egbuniwe, B. Leonhardt, Operational Aspects of a Biopolymer Flood in a Mature Oilfield presented at the SPE Improved Oil Recovery Symposium, SPE Improved Oil Recovery Symposium, Tulsa Oklahoma, USA, 12th–16th April, Society of Petroleum Engineers, 2014. DOI:SPE-169158-MS
9. Aseem A. T. Pandey, Milena Trifkovic, S. Bryant, Cellulose Nanocrystal Sta- bilized Emulsions for Conformance Control and Fluid Diversion in Porous Media presented at the SPE Annual Technical Conference and Exhibition, 24th–26th September 2018, Dallas, Texas, USA, Society of Petroleum Engin- eers, 2018. DOI:SPE-191609-MS
10. A. Yudhowijoyoa, R. Rafati, A. S. Haddad, D. Pokrajac, M. Manzari, De- veloping

Nanocomposite Gels from Biopolymers for Leakage Control in Oil and Gas Wells presented at the SPE Offshore Europe Conference and Ex- hibition, Aberdeen, UK, September, Society of Petroleum Engineers, 2019. DOI:SPE-195765-MS

11. M. Shamlooh, A. Hamza, I. A. Hussein, M. S. Nasser, S. Salehi, Reinforce- ment of Polyacrylamide-Co-Tert-Butyl Acrylate Base Gel Using Nanosilica for Conformance Control at Low and High Reservoir Temperatures presented at the SPE International Conference and Exhibition on Formation Damage Control, Lafayette, Louisiana, USA, February, Society of Petroleum Engin- eers, 2020. DOI:SPE-199324-MS
12. I. Lakatos, G. Szentes, A. Vago, Z. Karaffa, Application of Nanoparticle Aided Silicate Reservoir Conformance Control Method at the Algyo Field, Hun- gary: Fundamentals and Case Histories presented at the Abu Dhabi Interna- tional Petroleum Exhibition & Conference held in Abu Dhabi, UAE, 13th–16th November, Society of Petroleum Engineers, 2017. DOI:SPE-188563-MS
13. M. Gutierrez, J. S. García, T. Y. Zafra, J. Rojas, R. M. Ortiz, H. I. Quintero, H. A. Garcia, In-Depth Water Conformance Control: Design, Implementation and Surveillance of the First Thermally Active Polymers Treatment TAP in a Colombian Field
14. A. Andrianov, J. Hou, E. Li, E. Liu, L. Yang, Full-Scale Implementation of Conformance Control by Nanospheres in Large Sandstone Oil Field presented at the PE Conference at Oman Petroleum & Energy Show, Muscat, Oman, March, Society of Petroleum Engineers, 2022. DOI:SPE-200227-MS
15. G. Flavien, R. Christophe, L. Lionel, T. Antoine, Offshore Polymer EOR In- jection Philosophies, Constrains and Solutions presented at the SPE Improved Oil Recovery Conference, Society of Petroleum Engineers, 2020. DOI:SPE- 200368-MS
16. https://petrowiki.spe.org/Microbial_enhanced_oil_recovery accessed 20.05.2021
17. J. Pu, B. Bai, A. Alhuraishawy, T. Schuman, Y. Chen, X. Sun, A Novel Re-Crosslinkable Preformed Particle Gel for Conformance Control in Extreme Heterogeneous Reservoirs presented at the SPE Annual Technical Conference and Exhibition, Dallas, Texas, 24th–26th September, Society of Petroleum Engineers, 2018. DOI:SPE-191697-MS
18. F. Jin, Q. Li, Y. Liu, W. Pu, C. Yuan, X. Yuan, C. Liu, Q. Chen, M. A. Varfolomeev, K. Li, Successful Field Application of Delayed Water-Swelling, Flexible Gel Particles for In-Depth Waterflood Conformance Improvement in Wide Spacing of Wells with High

Temperature and High Salinity presented at the Abu Dhabi International Petroleum Exhibition & Conference,Abu Dhabi, UAE, 15th–18th November, Society of Petroleum Engineers, 2021. DOI:SPE- 207974-MS

19. A. Imqam, H. Elue, F. A. Muhammed, B. Bai, Hydrochloric Acid Applications to Improve Particle Gel Conformance Control Treatment presented at the SPE Nigeria Annual International Conference and Exhibition held in Lagos, Nigeria, 05th–07th August, Society of Petroleum Engineers, 2014. DOI:SPE- 172352-MS
20. B. Bai, X. Sun, Development of Swelling-Rate Controllable Particle Gels to Control the Conformance of CO2 Flooding presented at the SPE Improved Oil Recovery Conference, Tulsa, Oklahoma, USA, 18th–22th August, Society of Petroleum Engineers, 2020. DOI:SPE-200339-MS
21. Y. Wu, K.-S. Wang, Z. Hu, B. Bai, P. Shuler, Y. Tang, A New Method for Fast Screening of Long-Term Thermal Stability of Water Soluble Polymers for Reservoir Conformance Control presented at the SPE Annual Technical Conference and Exhibition, New Orleans, Louisiana, USA, 4th–7th October Society of Petroleum Engineers, 2009. DOI:SPE-124257
22. Z. Wang, B. Bai, Y. Long, L. Wang, SPE Journal 2019, , 2398–2408.
23. B. Weia, S. Chen, Q. Tian, J. Lu, X. Xu, SPE Reservoir Evaluation & En- gineering 2019, , 1219–1232.
24. C. L. Gaol, Investigation of Pore-scale Mechanisms of Microbial Enhanced Oil Recovery (MEOR) using a Microfluidics Approach, Papierflieger Verlag, Clausthal-Zellerfeld, 2020. ISBN:978-3-86948-777-9
25. K. M. Rankin, Novel Solvent Injection and Conformance Control Technologies for Fractured Viscous Oil Reservoirs, The University of Texas at Austin, The University of Texas at Austin, Austin, Texas, USA, 2013. ISBN:
26. K. Raney, S. Ayirala, P. Verbeek, Surface and Subsurface Requirements for Successful Implementation of Offshore Chemical Enhanced Oil Recovery presented at the , Society of Petroleum Engineers, 2012. DOI:SPE-155116-PA
27. N. Klueglein, F. Kögler, I. J. Adaktylou, M. L. Wuestner, E. Mahler, J. Scholz, A. Herold, H. Alkan, Understanding Selective Plugging and Biofilm Forma- tion of a Halophilic Bacterial Community for MEOR Application presented at the SPE Improved Oil Recovery Conference, 11th–13th April 2018, Tulsa, Oklahoma, USA, Society of Petroleum Engineers, 2018. DOI:SPE-179620-MS

28. J. Vasquez, R. Curtice, A Porosity-Fill Sealant for Water and Gas Shutoff: Case Histories and Lessons Learned after more than 1 000 Well Interven- tions presented at the SPE European Formation Damage Conference and Ex- hibition, 5-7 June, Noordwijk, Netherlands, Society of Petroleum Engineers, 2013. DOI:10.2118/165090-MS
29. J. Vasquez, D. Tuck, Environmentally Acceptable Porosity-Fill Sealant Sys- tems for Water and Gas Control Applications presented at the SPE Latin American and Caribbean Health, Safety, Environment and Sustainability Conference, 7-8 July, Bogotá, Colombia, Society of Petroleum Engineers, 2015. DOI:10.2118/174098-MS
30. E. Anglaret, A. Hasmy, R. Jullien, Phys. Rev. Lett. 1995, 175, 14059.
31. J. Vasquez, L. Eoff, A Relative Permeability Modifier for Water Control: Candidate Selection, Case Histories, and Lessons Learned after more than 3 000 Well Interventions presented at the SPE European Formation Dam- age Conference and Exhibition, 5-7 June, Noordwijk, Netherlands, Society of Petroleum Engineers, 2013. DOI:10.2118/165091-MS
32. Exploring shortest paths – part 5. Available online: https://blogs.mathworks.com/steve/2011/12/13/exploring-shortest-paths- part-5/ (accessed on 15 February 2022).
33. Warning: citation key “GaolPhD” is not in the bibliography database.

Abbreviations

BH	Bentheimer
CC	concentric cylinder
Dβ	Dogger β
DG	double gab
EOR	Enhanced Oil Recovery
IOR	Improved Oil Recovery
KCl	potassium chloride
NaCl	sodium chloride
PAtBA	polyacrylamide *tert*-butyl acrylate
PEI	polyethylenimine
PP	parallel plate
PV	pore volume
RPM	relative permeability modifier
TVI	total volume injected

Symbols and units

Symbols

λ_i	phase mobility
μ_i	dynamic viscosity at a shear rate of i s^{-1}
μ	dynamic viscosity
ϕ	porosity
c	concentration
d	diameter
k_i	effective permeability
k	permeability
l	length
M	mobility ratio
T_g	gelation temperature
T	temperature
t_G	gelation time

Units

°C	degree Celcius
mD	millidarcy
g	gramm
h	hours

L	litre
µL	microliter
mL	millilitre
m	metre
µm	micrometre
mm	millimetre
cm	centimetre
Pa	pascal
ppm	parts per billion
ppm	parts per million
ppm	round per minute
s	seconds

Appendix

*Table 23: **A1:** Gel strength by Sydansk*

Gel strength	Definition	Description
A	No detectable gel formed	The gel appears to have the same viscosity
B	Highly flowing gel	The gel appears to be only slightly more
C	Flowing gel	Most of the obviously detectable gel flows to the bottle cap upon inversion.
D	Moderately flowing gel	A small portion (about 5 to 15 %) of the gel does not readily flow to the bottle cap upon inversion. This is usually characterized as a “tonguing” gel (after hanging out of the bottle, gel can be made to flow back into the bottle by slowly turning the bottle upright).
E	Barely flowing gel	The gel slowly flows to the bottle cap and/or
F	Highly deformable nonflowing gel	The gel does not flow to the bottle cap upon inversion (gel flows to just short of reaching the bottle cap).
G	Moderately deformable nonflowing gel	The gel flows about halfway down the bottle upon inversion
H	Slightly deformable nonflowing gel	Only the gel surface deforms slightly upon inversion.
I	Rigid gel	There is no gel-surface deformation upon inversion.
J	Ringing rigid gel	A tuning-fork-like mechanical vibration can be felt after the bottle is trapped.

www.dgmk.de